J-11.5 Removing the Production Wells

The following simulations are presented to evaluate the potential land-use impact which affects the amount of water required and the time-frame during which it is required. In the RI/BRA, it was assumed that the land-use through year 2095 would require pumping water from the SRPA at current rates. This assumption is consistent with an industrial use scenario, where large water volumes would be necessary in order to sustain the commercial activities. If the land-use changes significantly, or if the current production wells are moved out of the influence of INTEC (i.e., further north or east), the draw-down currently observed in the aquifer would stop. The influence of the production wells will be shown relative to the drawdown predicted for the RI/BRA base case in year 2010 (Figure J-11-47). Important features in Figure J-11-47 include the (a) locations of the CPP-2 and CPP-1 production wells just south of the INTEC fence line, (b) position of the 1356.4 m and 1356.6 m contour lines, and the very flat head distribution between them, and (c) the head gradient overall represented by the density of contours drawn at 0.1 m contour intervals.

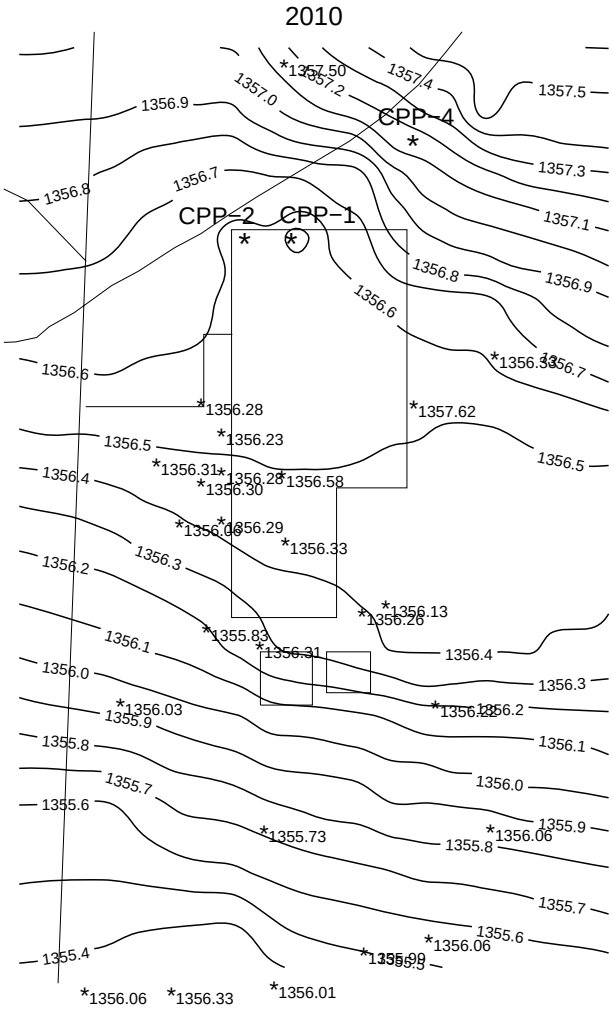

Figure J-11-47. Head (m) distribution predicted for the RI/BRA base case in year 2010.

J-11.5.1 Removing the Production Wells in 2012.

In the simulation presented below, pumping from CPP-1 and CPP-2 is assumed to stop in year 2012. Because the land-use scenario remains potentially industrial, the anthropogenic water losses were not reduced in this simulation, making this simulation representative of relocating the production wells outside of the INTEC viscinity. This simulation uses the activity-flux from the alluvium corresponding to the RI/BRA base case discussed in Section J-8.1, and also uses the RI/BRA flux of Sr-90 out of the vadose zone. As a result, the differences between the RI/BRA model predictions and those presented below are the sole consequence of production in the CPP-1 and CPP-2 wells.

J-11.5.1.1 Aquifer Sr-90 Simulation Results

After removal of the production wells, the hydraulic head almost immediately returns to pre-pumping conditions. The affect of the production wells on the hydraulic head is apparent through the comparison of Figures J-11-47 and J-11-48. The hydraulic influence of the production wells is obvious. Important features to note include the

- shift southward of the 1356.4 m and 1356.6 m contour lines. In the RI/BRA model, the 1356.6 m level occurred north of the two production wells, and the 1356.4 m contour level was south of the CPP-3 injection well. After removing the production wells, the lower contour passes just north of the former percolation ponds, and the 1356.6 m contour level is about where the 1356.5 m contour level was in the RI/BRA model. This implies that the region of influence of the pumping wells extends well south of the former percolation ponds. Differences in contour levels exist well north of the production wells.
- absence of the very flat head distribution in central INTEC. Removing the production wells has greatly increased the gradient in the region containing the highest predicted concentrations in the INTEC facility boundary. This means that the velocity in that region will be proportionally higher.
- drawdown north of the tank farm toward CPP-1 and CPP-2. It is known that the production wells are capturing contaminants (ICP 2004). In the 110-ft interbed, there is a water divide caused by a change in slope that occurs very near the tank farm. North of the tank farm, the interbed slopes toward the Big Lost River, and South of the tank farm, the slope is to the south. It is likely that contaminants being produced in CPP-1 and CPP-2 are coming from the vadose zone, and that those produced contaminants are associated with flow to the north of the divide.
- width of the area affected by the production wells near CPP-1 and CPP-2. Pumping alternates between CPP-1 and CPP-2. This switching contributes to northwestward movement of water and contaminants, increased dispersion, intermittant southward transport, and very slow transport in the aquifer of contaminants arriving from the vadose zone northeast of the tank farm.
- head gradient overall. The gradient northeast of the production wells and the gradient south of the former percolation ponds is very similar in both models. This suggests that the migration of Sr-90 currently in the SRPA and south of the former percolation ponds will not be affected by removing the production wells. However, it is clear that there will be some influence within the facility boundaries.

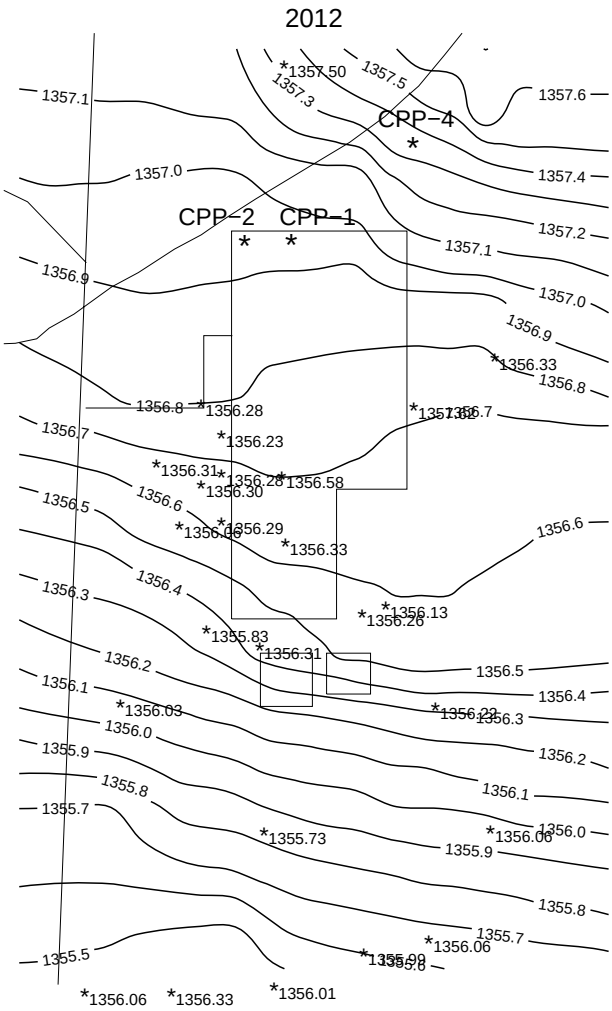

Figure J-11-48. Head (m) distribution predicted after removing the production wells in year 2012.

The influence on Sr-90 transport is shown in the far-field for the time period spanning 2005-2096 in Figure J-11-49. The near-field distribution is shown in Figure J-11-50 for the 2049-2151 time period, and resultant peak aquifer concentrations are given in Figure J-11-51. Comparing the far-field distribution of Sr-90 shows that removing the production wells has little effect on the distribution of Sr-90 downgradient of INTEC through year 2022. This is primarily because the Sr-90 currently in the aquifer was introduced in well CPP-03 which is in the region of the aquifer least affected by the imposed pumping gradients. In the near-field, the area impacted above the MCL is much smaller in central INTEC by year 2049. Increased velocity through central INTEC allows for more dilution and increased dispersion. Although natural attenuation is increased, it still is not sufficient to completely counter the incoming fluxes from the vadose zone. To the northeast of the tank farm, a small region above the MCL has developed. The increase in concentrations near the production wells is a result of (a) decreasing the dispersion that was being caused by switching production between the two wells, and (b) removing the slight remediation that occurs during the pumping operations.

Peak aquifer concentration decreases immediately after pumping ceases from the production wells. However, the peak concentrations are again very similar by year 2150. The convergance of peak concentration occurs because the location of the peak concentration is different with and without the production wells present. By year 2108, predicted concentrations are below the MCL, and by year 2095, the peak concentration is 11.9 pCi/L. Relocating the production wells has reduced the time during which the MCL is exceeded by 20 years. This is significant from the perspective of contingent pump and treat alternatives being evaluated in the feasibility study.

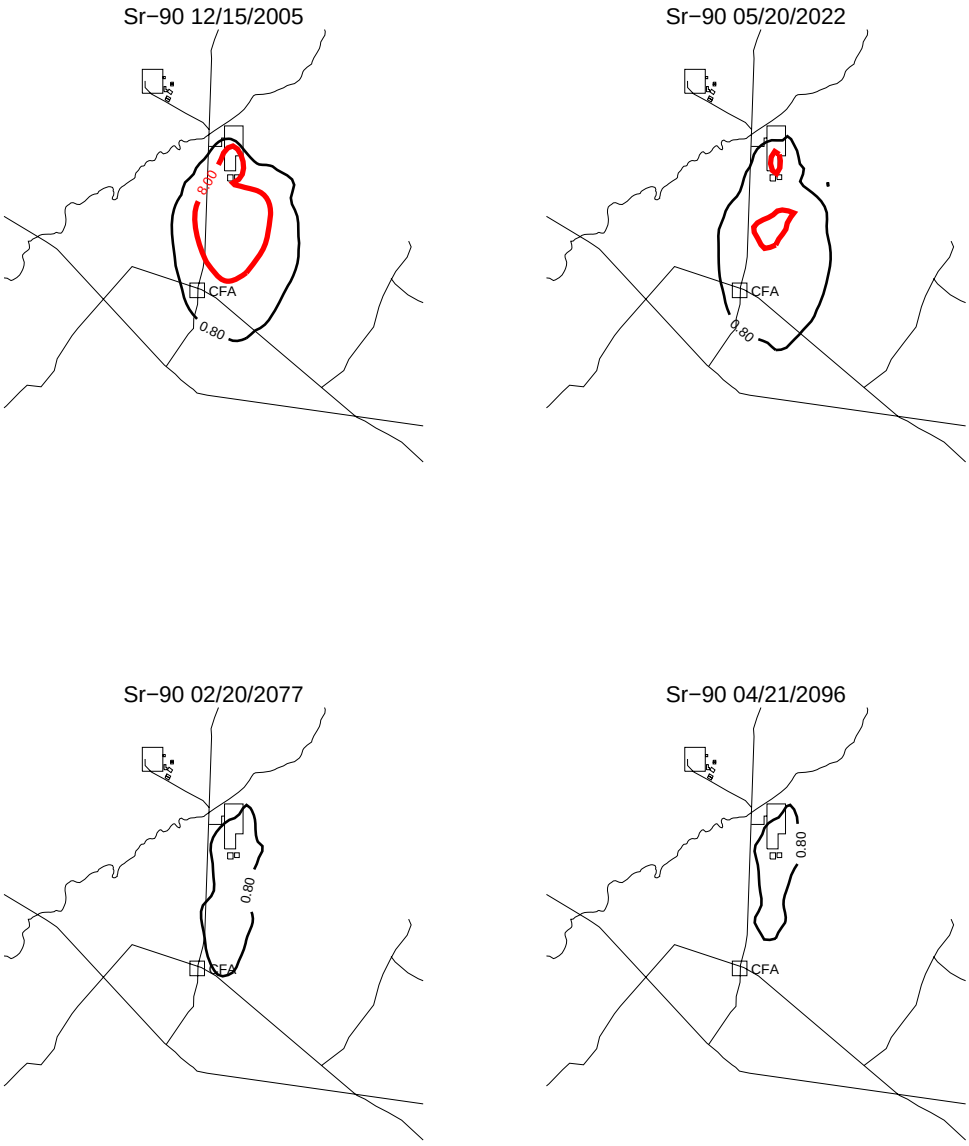

Figure J-11-49. Sr-90 aquifer concentration contours removing production wells in 2012 (pCi/L) (MCL = thick red line, 10*MCL = thin red line, MCL/10 = black line).

Figure J-11-50. Sr-90 aquifer concentration contours removing production wells in 2012 (pCi/L) (continued) (MCL = thick red line, 10*MCL = thin red line, MCL/10 = black line).

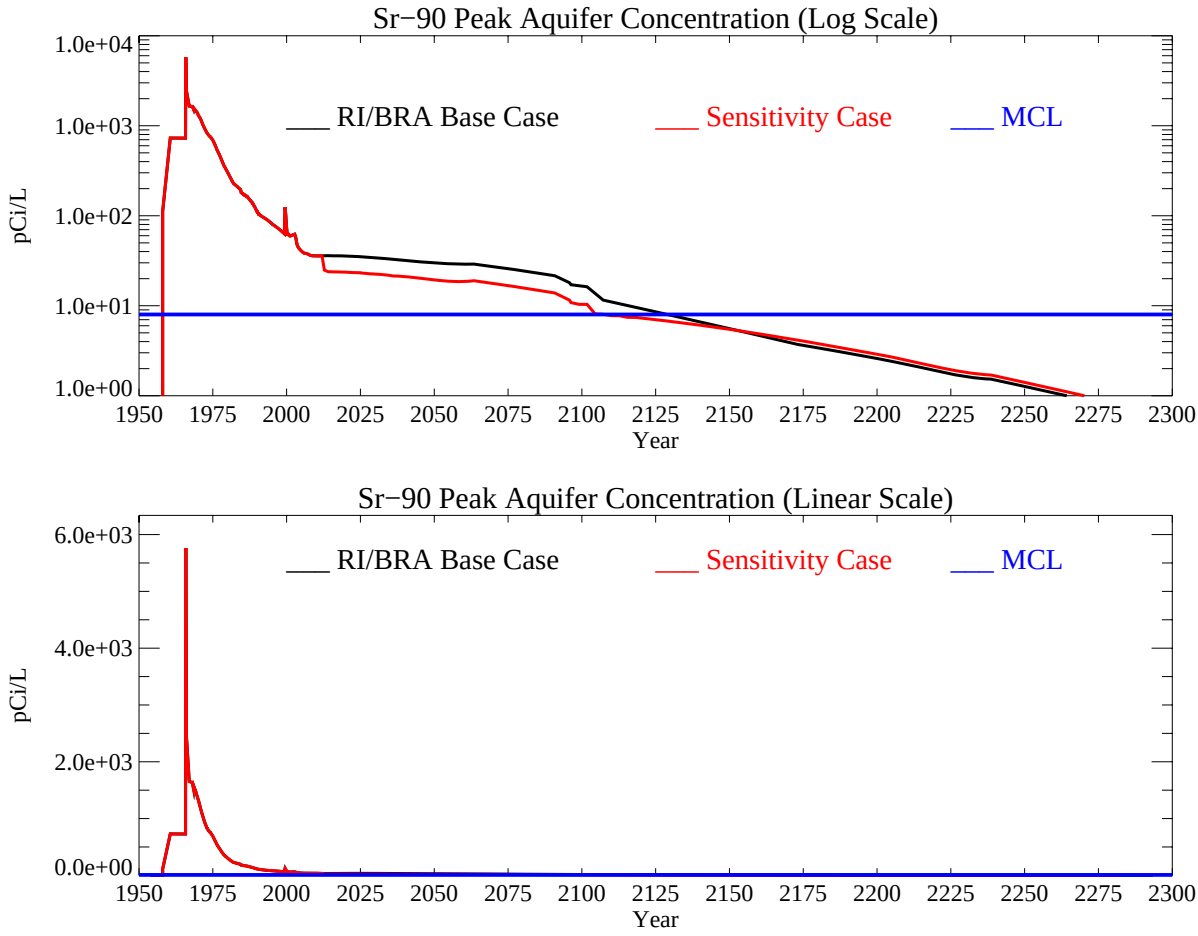

Figure J-11-51. Sr-90 peak aquifer concentrations removing production wells in 2012 (pCi/L) with the MCL shown in blue, the RI/BRA model in black and this sensitivity run in red.

J-11.5.2 Removing the Production Wells In Year 2035

In the simulation presented below, pumping is assumed to stop in year 2035. This simulation uses the activity-flux from the alluvium corresponding to the RI/BRA base case discussed in Section J-8.1, and also uses the RI/BRA flux of Sr-90 out of the vadose zone. Because the land-use scenario remains potentially industrial, the anthropogenic water losses were not reduced. Thus, this simulation is representative of relocating the production wells outside of the INTEC viscinity.

J-11.5.2.1 Aquifer Sr-90 Simulation Results

The effect of the production wells in year 2035 is very similar to that in year 2012. This is apparent by comparing the hydraulic head in Figures J-11-48 and J-11-52. The similar hydraulic influence occurs because:

- steady-state Big Lost River recharge is assumed to start in year 2005, and was in effect prior to year 2012 and through the end of the simulation period.
- precipitation recharge is steady-state throughout the simulation period.
- transient fluxes equilibrated prior to year 2012 after the percolation ponds were relocated.
- the equilibration period in the aquifer is extremely short after the production wells are turned off.

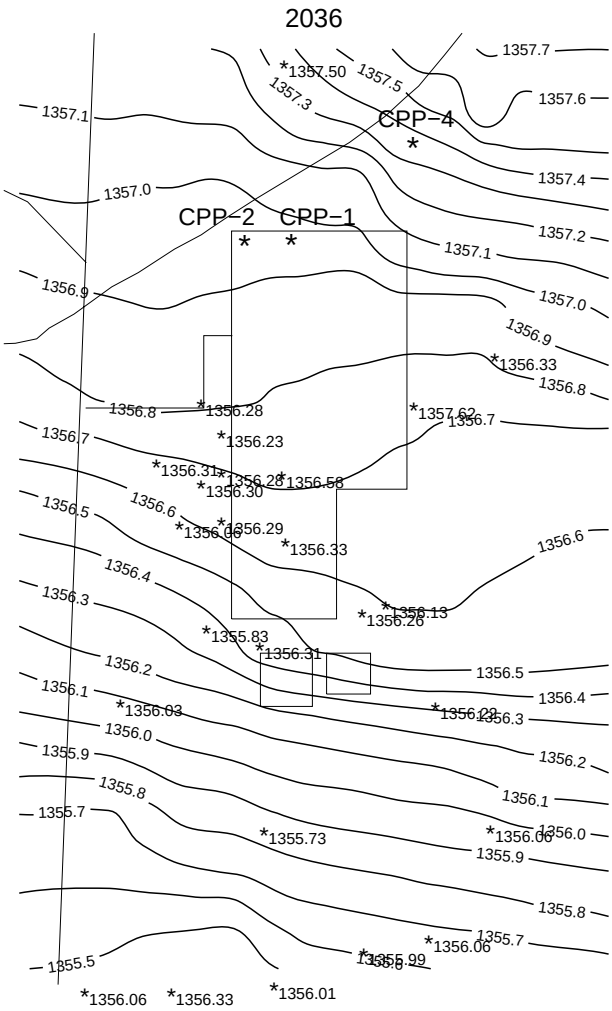

Figure J-11-52. Head (m) distribution predicted after removing the production wells in year 2035.

The influence on Sr-90 transport is shown in the far-field for the time period spanning 2005-2096 in Figure J-11-53 with the near-field distribution shown in Figure J-11-54 for the 2049-2151 time period. Resultant peak aquifer concentrations are given in Figure J-11-55. Because the water flux from the vadose zone is steady-state after year 2012, the incoming fluxes are exactly the same in all of the production well sensitivity simulations. The continual arrival from the vadose zone is being attenuated in the aquifer at rate sufficient to keep the Sr-90 plume within the INTEC fence regardless of whether or not the production wells are in use. Removing the production wells 20 years earlier allowed those fluxes to be attenuated for a longer period of time, but the continued arrival keeps concentrations above the MCL through year 2107 in either case, and the peak concentrations (11.9 pCi/L) in year 2095 are nearly identical.

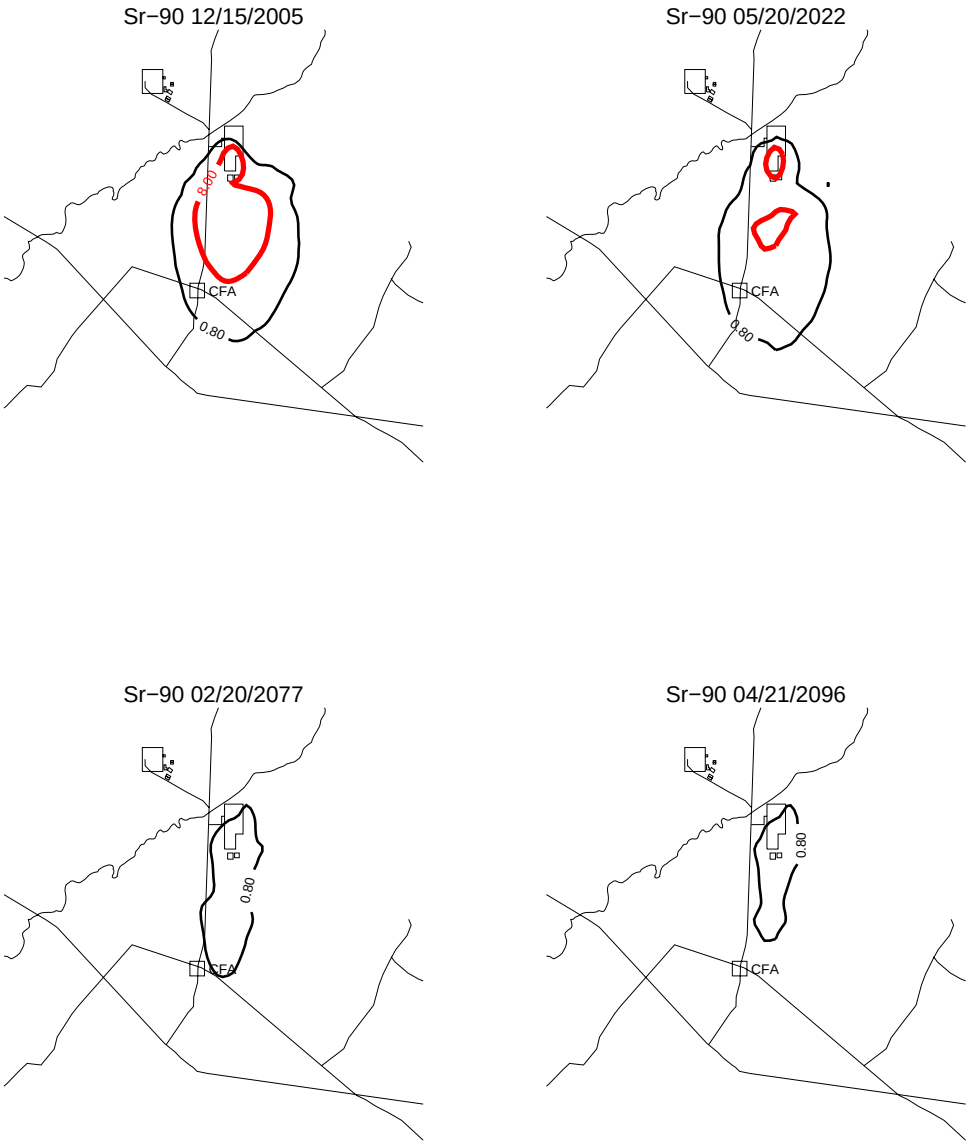

Figure J-11-53. Sr-90 aquifer concentration contours removing the production wells in 2035 (pCi/L) (MCL = thick red line, 10*MCL = thin red line, MCL/10 = black line).

Figure J-11-54. Sr-90 aquifer concentration contours removing the production wells in 2035 (pCi/L) (continued) (MCL = thick red line, 10*MCL = thin red line, MCL/10 = black line).

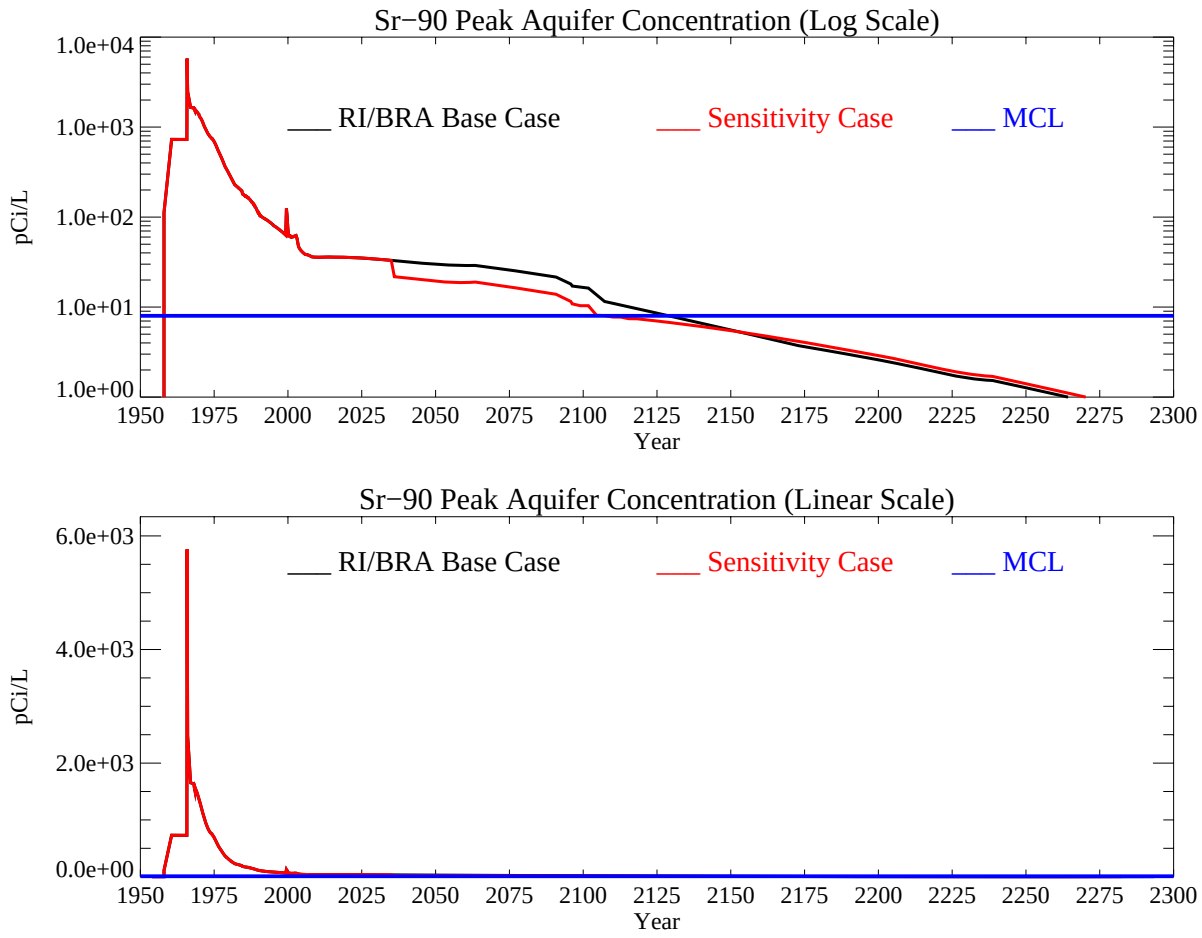

Figure J-11-55. Sr-90 peak aquifer concentrations removing the production wells in 2035 (pCi/L) with the MCL shown in blue, the RI/BRA model in black and this sensitivity run in red.

J-11.5.3 Removing the Production Wells In Year 2096

In the simulation presented below, pumping is assumed to stop in year 2096. This simulation uses the activity-flux from the alluvium corresponding to the RI/BRA base case discussed in Section J-8.1, and also uses the RI/BRA flux of Sr-90 out of the vadose zone. Because the land-use scenario remains potentially industrial, the anthropogenic water losses were not reduced. Thus, this simulation is representative of relocating the production wells outside of the INTEC viscinity.

J-11.5.3.1 Aquifer Sr-90 Simulation Results

After removal of the production wells, the hydraulic head almost immediately returns to pre-pumping conditions. The affect of the production wells in year 2096 is again very similar to that in years 2012 and 2035. This is apparent by comparing the hydraulic head in Figures J-11-48, J-11-52, and J-11-56. The similarity in hydraulic influence occurs because:

- steady-state Big Lost River recharge is assumed to start in year 2005, and was in effect prior to year 2012 and through the end of the simulation period.
- precipitation recharge is steady-state throughout the simulation period.
- transient fluxes equilibrated prior to year 2012 after the percolation ponds were relocated.
- the equilibration period in the aquifer is extremely short after the production wells are turned off.

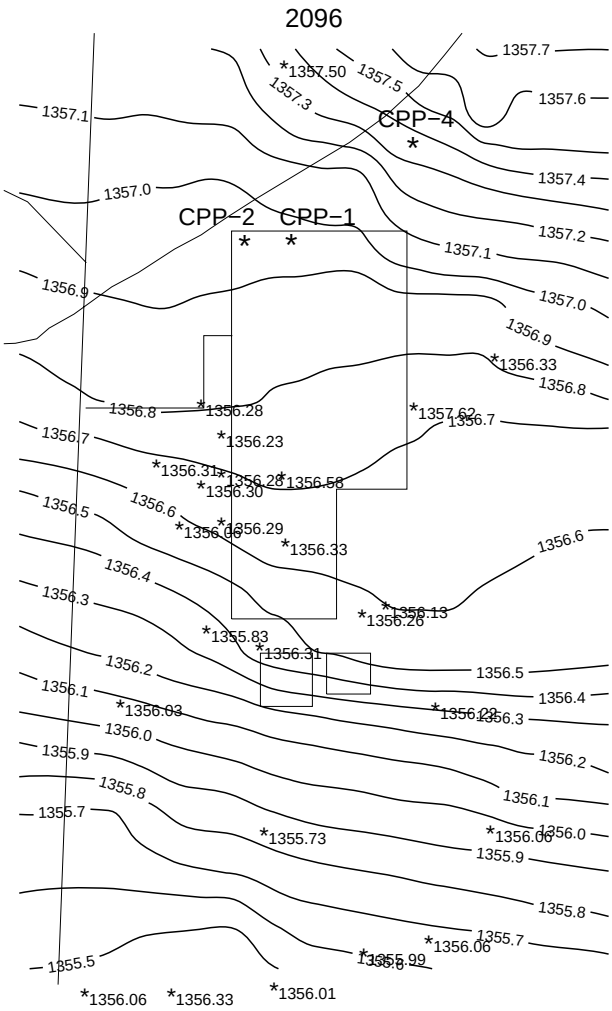

Figure J-11-56. Head (m) distribution predicted after removing the production wells in year 2096.

The influence on Sr-90 transport is shown in the far-field for the time period spanning 2005-2096 in Figure J-11-57 with the near-field distribution shown in Figure J-11-58 for the 2049-2151 time period. Resultant peak aquifer concentrations are given in Figure J-11-59. Waiting until year 2097 to remove the production wells has a slight impact on the distribution of Sr-90 above the MCL. Removing the production wells in either 2012 or 2035 allowed earlier natural attenuation of Sr-90 to occur in central INTEC, but keeping the production wells on-line through year 2096 prevents concentrations above the MCL from occurring in northeast INTEC. Because the water flux from the vadose zone is steady-state after year 2012, the incoming fluxes are exactly the same in all of the production well sensitivity simulations. Removing the production wells earlier allows those fluxes to be attenuated for a longer period of time. However, the peak aquifer concentration still exceeds the MCL through year 2108 and is 18.6 pCi/L in year 2096.

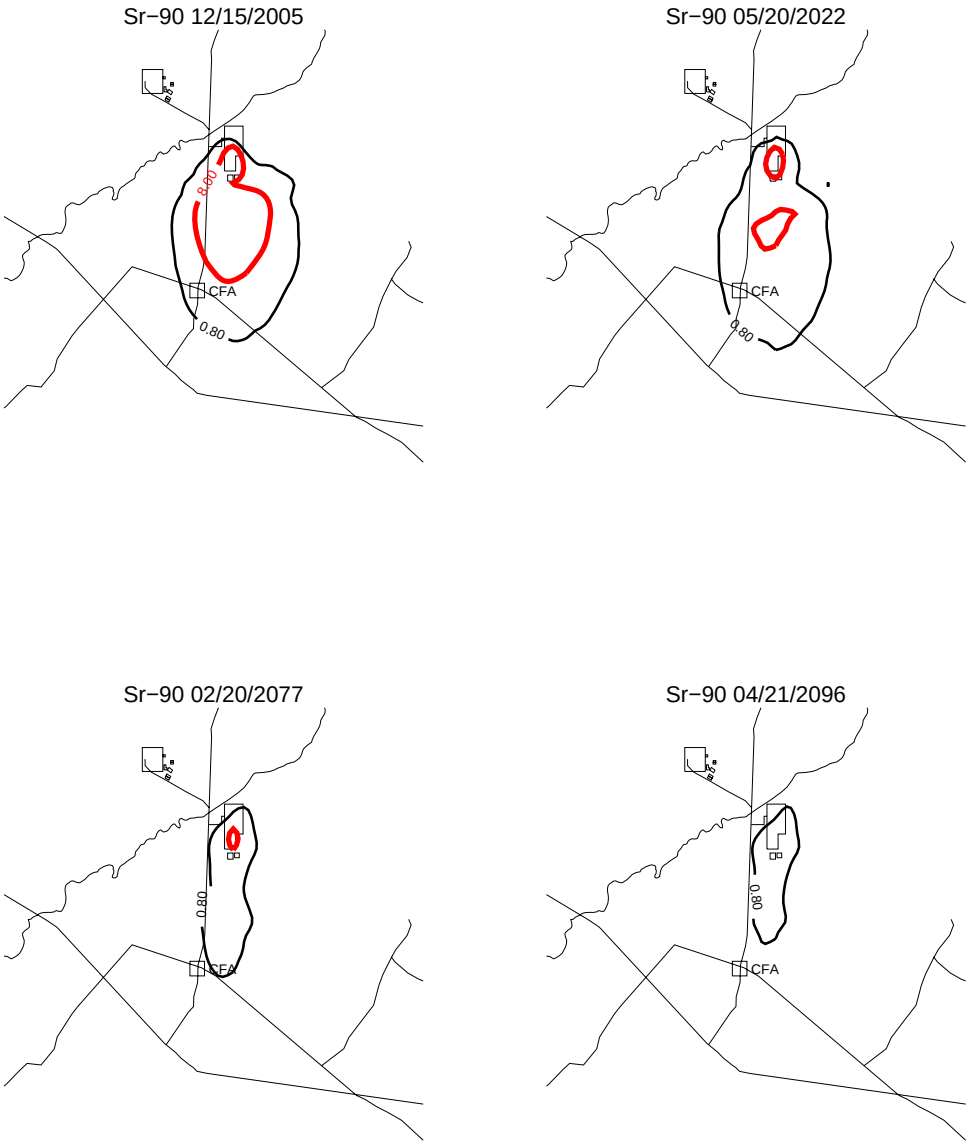

Figure J-11-57. Sr-90 aquifer concentration contours removing the production wells in 2096 (pCi/L) (MCL = thick red line, 10*MCL = thin red line, MCL/10 = black line).

Figure J-11-58. Sr-90 aquifer concentration contours removing the production wells in 2096 (pCi/L) (continued) (MCL = thick red line, 10*MCL = thin red line, MCL/10 = black line).

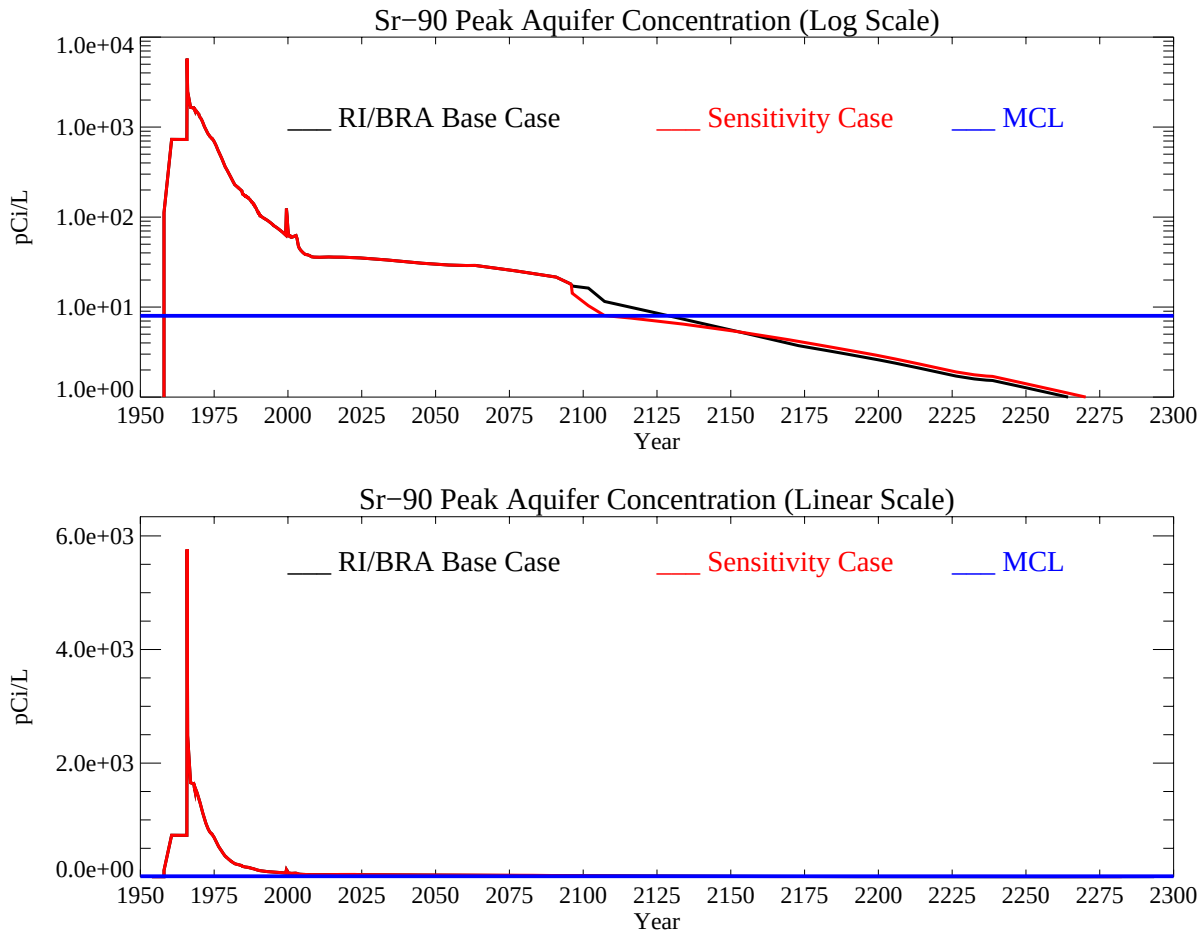

Figure J-11-59. Sr-90 peak aquifer concentrations removing the production wells in 2096 (pCi/L) with the MCL shown in blue, the RI/BRA model in black and this sensitivity run in red.

J-11.6 Larger Interbed Dispersivity

Dispersion is used to account for solute transport that occurs in addition to pure advection. In theory, it is the result of different flow velocities affecting the transport of solute particles moving through porous media. Assuming Fickian dispersion, this process will spread the solute in all directions. The amount of dispersion that occurs is a function of the heterogeneity of the media, the advective velocity, media porosity, water saturation, and concentration gradient. As a single measure, dispersivity tends to be a scale dependent phenomena with the magnitude on the order of 10% of the domain of interest in saturated groundwater systems, with decreasing dispersivity as the transport distance increases (Gelhar, 1986). In numerical models, advection and dispersion are accounted for through the implementation of the advective-dispersion transport equations. In addition, dispersion is introduced through spatial and temporal discretization. This later dispersion is model dependant, or dependant on the specific implementation incorporated in a given numerical code. As a result, a specific value for dispersivity has little actual meaning, but when incorporated into the simulation process, becomes a model fitting parameter. Fitting this parameter is done by first selecting a numerical model, gridding the system in time and in space, and by matching predicted concentration histories to measured field data for the transport of conservative (non-reacting) species. In other words, it becomes a calibration target.

The degree to which the final total model matches observed transport of Tc-99, H-3, and I-129 is a reflection of the complete calibration. In all of these cases, the observed perched water data was incomplete. Data was not collected early enough in time to capture the initial arrival of contaminants, the rise to peak concentrations, or the tailing off of the concentration history. A best-fit model was calibrated to those contaminants based on the available data. As a result, there is uncertainty in the derived model dispersivity.

The base grid vadose zone model used a 1 m longitudinal and 0.1 m transverse dispersivity. Larger dispersivity values can significantly affect peak aquifer concentrations for strongly sorbing and short lived contaminants such as Sr-90, where the bulk of the contaminant decays in the vadose zone because of sorption. The dispersive component increases the net transport, but reduces the aqueous phase concentration, and results in more of the contaminant being adsorbed on porous media. Although the dispersivity used in the RI/BRA model was derived for conservative tracers, looking at the sensitivity for Sr-90 is important. A larger dispersivity might allow lateral transport toward the MW-33-1 and MW-55-06 wells that are consistently being under predicted while dropping concentrations in wells that are consistently overpredicted nearer the tank farm. Transport sensitivity for Sr-90 to dispersivity in the vadose zone is evaluated here by increasing the longitudinal dispersivity to 15 m and increasing the transverse dispersivity to 1.5 m, values that are roughly 10% of the horizontal and vertical model dimensions.

J-11.6.1 Vadose Zone Sr-90 Simulation Results

Figures J-11-60 through J-11-63 illustrate the distribution of the Sr-90 in the vadose zone through the year 2293. The effect of increased dispersivity is very apparent in the contour plots presented for the vertical plain in years later than 2000. Increasing the dispersivity spreads the higher concentrations laterally above the 140 ft interbed. It affects sources in northern and southern INTEC, and allows the Sr-90 from both sources to merge in central INTEC.

Figure J-11-64 illustrates Sr-90 arrival in key perched water wells, and the comparison to field data is summarized for all of the perched water wells in Figure J-11-65. The subplots presented in Figure J-11-64 show that the model is better predicting concentrations in wells 33-1, MW-10-2, MW-18-1, MW-20-2, PW-2, PW-4, and USGS-50. Well 33-1 is just south of the tank farm, and the remainder of the better matches occur near the former percolation ponds. In the higher concentration wells near the tank farm, although increasing the dispersivity allows more lateral migration (needed to push the Sr-90 to the south and east), it also results in more adsorption and overall lower concentrations. The resulting effect is underpredicting concentrations in

those key wells. The plots of RMS suggest that the overall mean RMS in this sensitivity case is better (lower mean RMS) than in some of the other parameter sets appearing in the overall sensitivity study. If the average RMS value were biased toward the wells in which the highest concentrations occur (field data), the average RMS would actually be much higher and would indicate a poorer overall match in the 110 ft and 140 ft interbeds.

Peak vadose zone concentrations through time are given in Figure J-11-66 for this simulation by the red line. The dispersivity tends to damp the peak concentration response, but in general, the predicted peak concentration is not significantly different from the RI/BRA base case concentrations (black) throughout most of the time period.

The rate at which Sr-90 enters the aquifer is given by the red line in Figure J-11-67, and can be compared directly to the RI/BRA base case (black). It is interesting to note that increasing the dispersivity has resulted in significantly lower fluxes into the aquifer during the 2000-2200 time period.

Figure J-11-60. Sr-90 vadose zone concentration with increased dispersivity (horizontal contours) (pCi/L) (MCL=thick red line, 10*MCL = thin red line, MCL/10 = dotted line).

Figure J-11-61. Sr-90 vadose zone concentration with increased dispersivity (horizontal contours) (pCi/L) (MCL=thick red line, 10*MCL = thin red line, MCL/10 = dotted line).

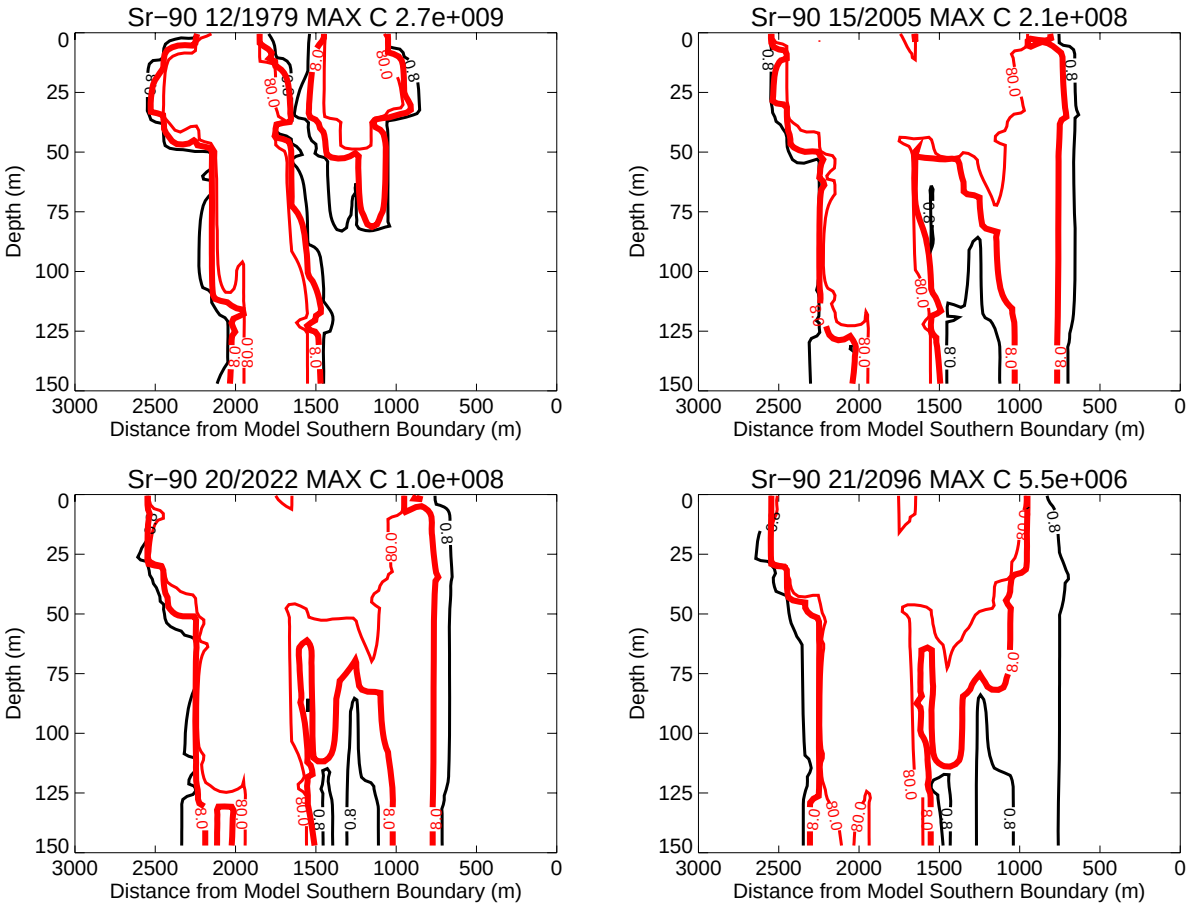

Figure J-11-62. Sr-90 vadose zone concentrations with increased dispersivity (vertical contours) (pCi/L) (MCL=thick red line, 10*MCL = thin red line, MCL/10 = dotted line).

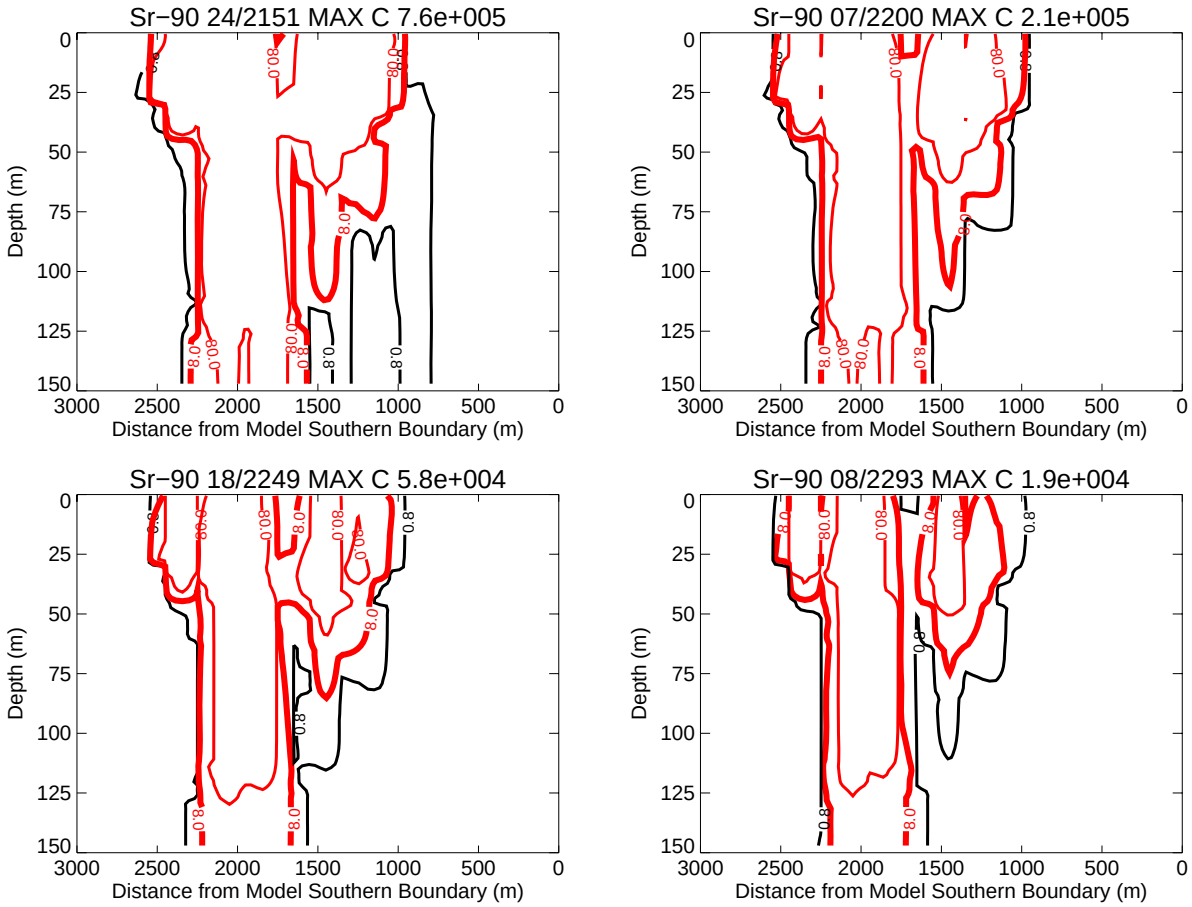

Figure J-11-63. Sr-90 vadose zone concentrations with increased dispersivity (vertical contours) (pCi/L) (continued) (MCL=thick red line, 10*MCL = thin red line, MCL/10 = dotted line).

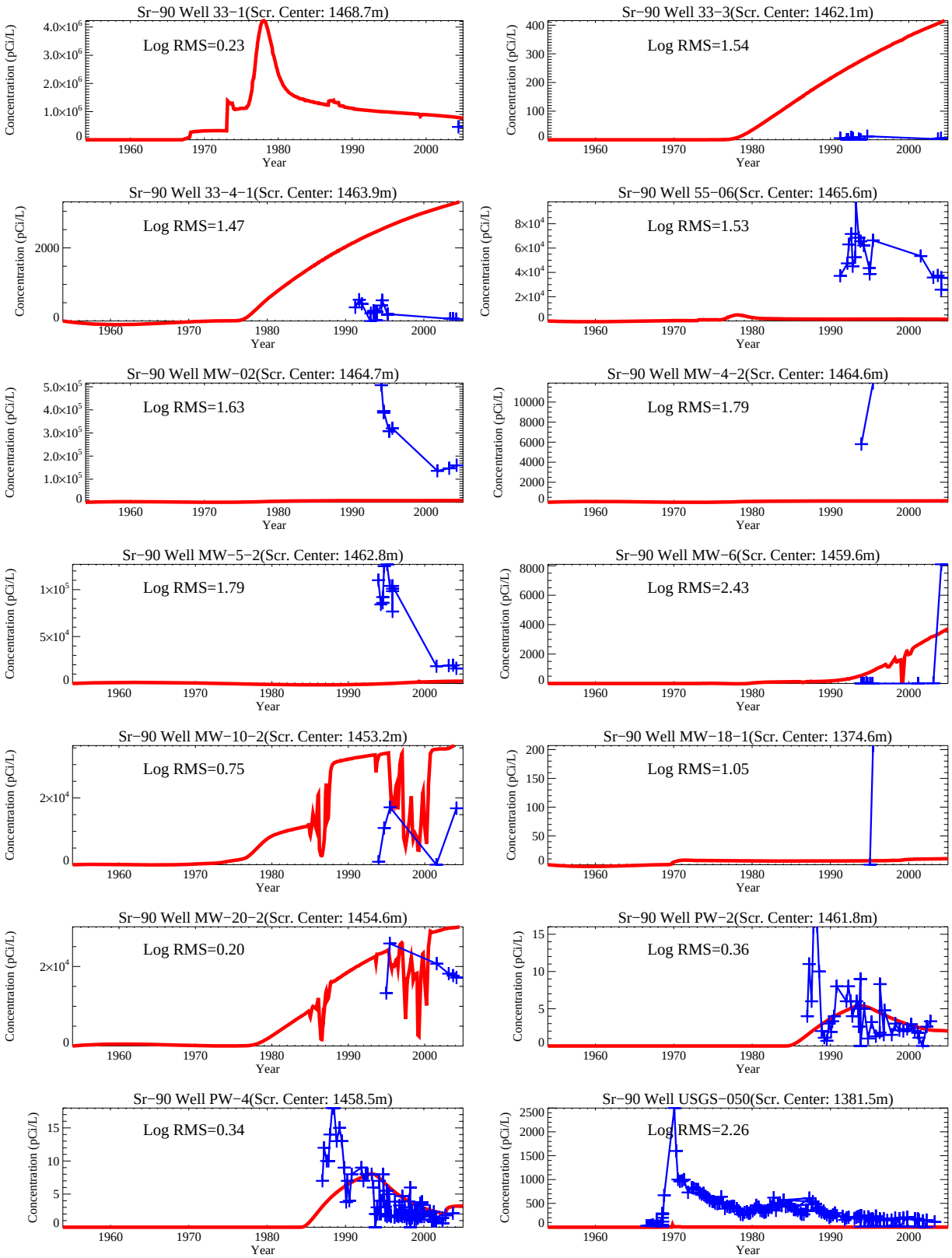

Figure J-11-64. Sr-90 concentration in perched water wells with increased dispersivity (pCi/L) (Measured values=blue crosses, Red=model at screen center).

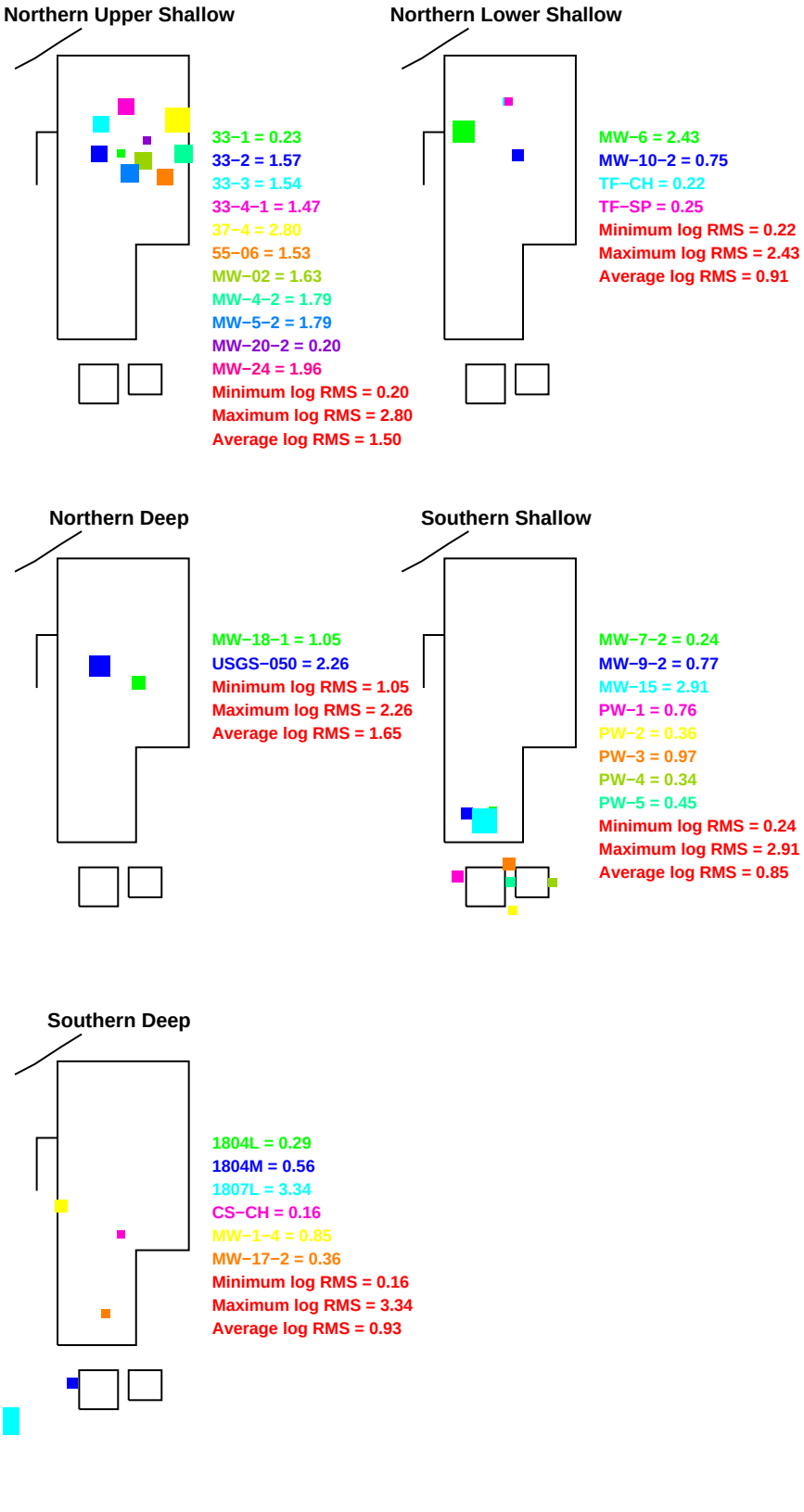

Figure J-11-65. Log 10 Root mean square error (RMS) by depth and northing with increased dispersivity.

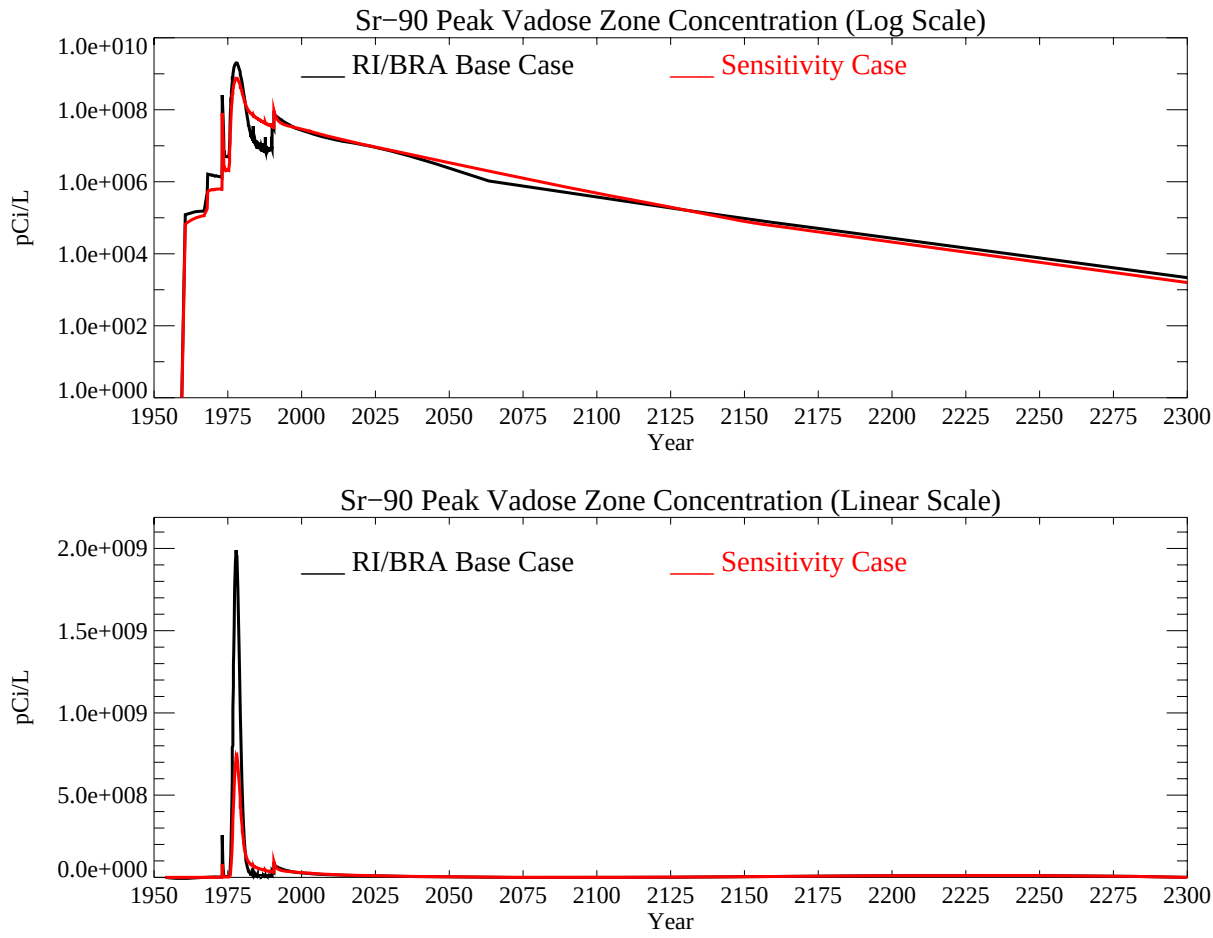

Figure J-11-66. Sr-90 peak vadose zone concentrations with increased dispersivity (pCi/L) The RI/BRA model is shown in black, and this sensitivity run in red.

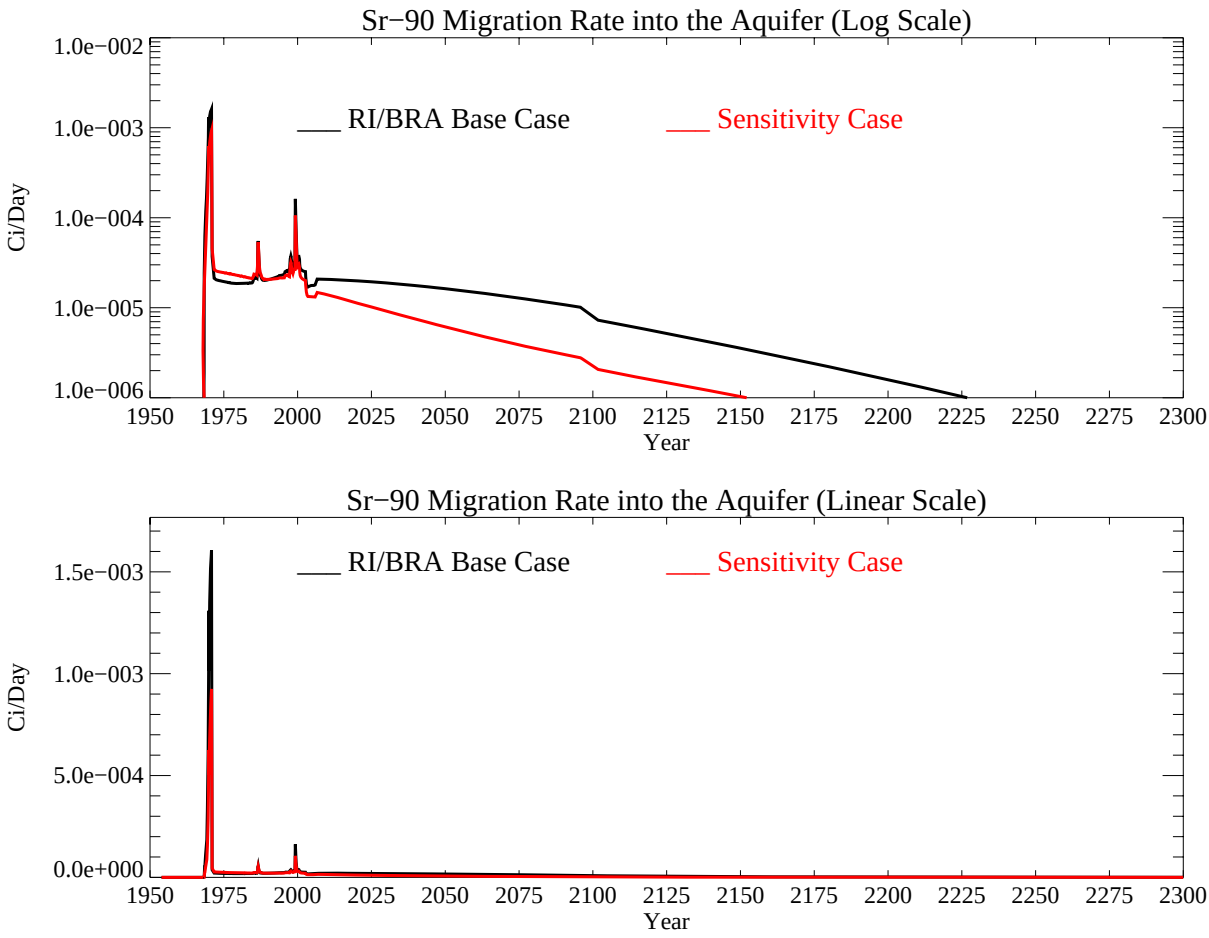

Figure J-11-67. Sr-90 activity flux into the aquifer with increased dispersivity (Ci/day). The RI/BRA model is shown in black, and this sensitivity run in red.

J-11.6.2 Aquifer Sr-90 Simulation Results

The distribution Sr-90 in the aquifer is given in Figures J-11-68 and J-11-69 contoured on the course and fine model grids, respectively. The area impacted by Sr-90 above the MCL is very similar to that predicted in the RI/BRA base case through year 2022. This area represents the long-term Sr-90 injection into the SRPA through the CPP-03 injection well. By year 2049, fluxes from the vadose zone arrive, and the decrease in flux rate is shown by the much smaller area enclosed by the 8 pCi/L contour line. As shown in Figure J-11-69, concentrations above the MCL are predicted to be between the former percolation ponds and the tank farm by year 2049.

The resultant peak aquifer concentrations are given in Figure J-11-70. With this increased dispersivity, the simulated Sr-90 concentrations are predicted to remain above the MCL from 1960 through year 2074. In year 2095, the predicted peak Sr-90 concentration is 4. pCi/L, about 21% of that predicted for the base case (18.6 pCi/L). During that period, the majority of the aquifer impact originates from direct injection rather than dispersive transport of Sr-90 from the tank farm.

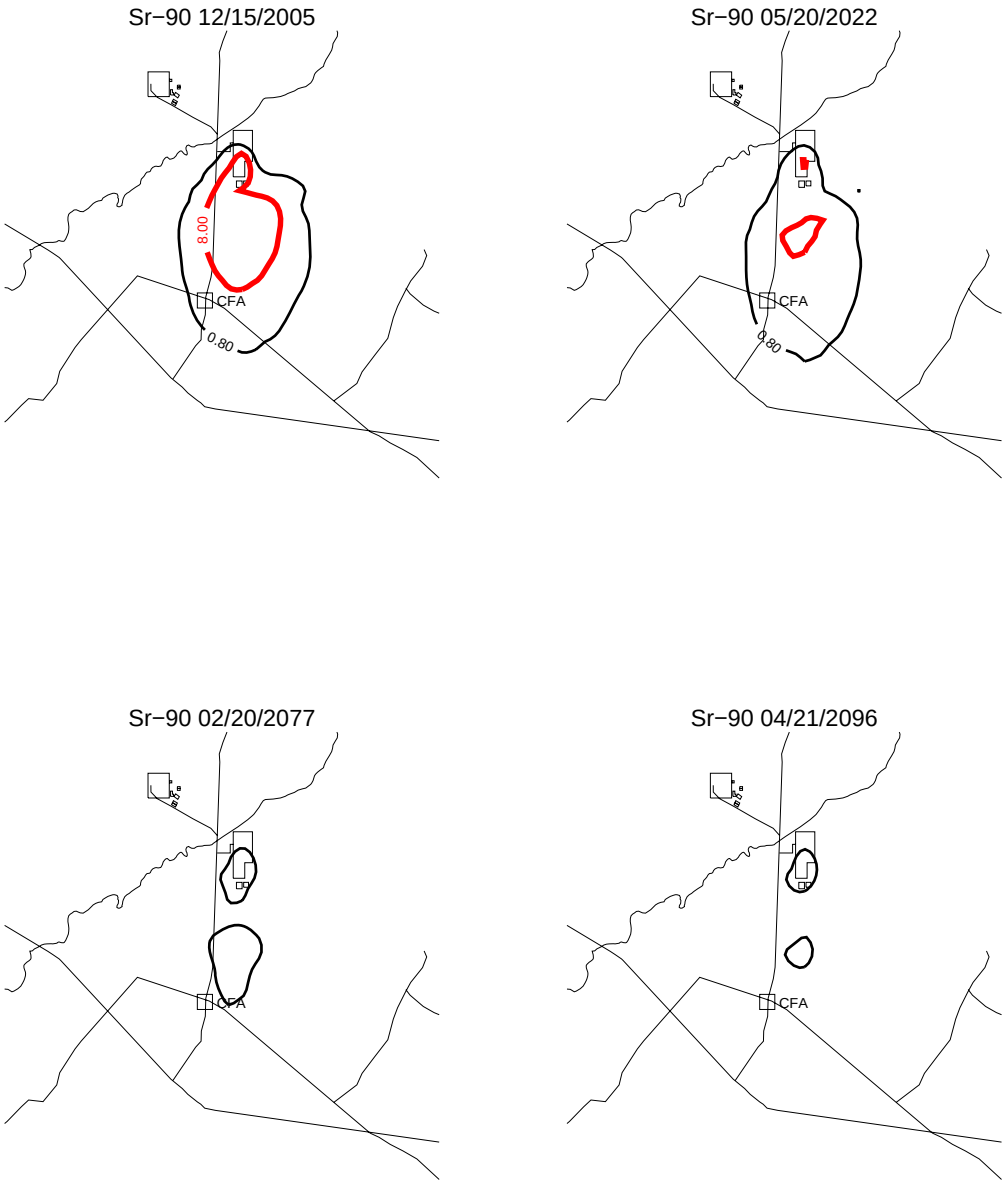

Figure J-11-68. Sr-90 aquifer concentration contours with increased dispersivity (pCi/L) (MCL=thick red line, 10*MCL = thin red line, MCL/10 = dotted line).

Figure J-11-69. Sr-90 aquifer concentration contours with increased dispersivity (pCi/L) (continued) (MCL=thick red line, 10*MCL = thin red line, MCL/10 = dotted line).

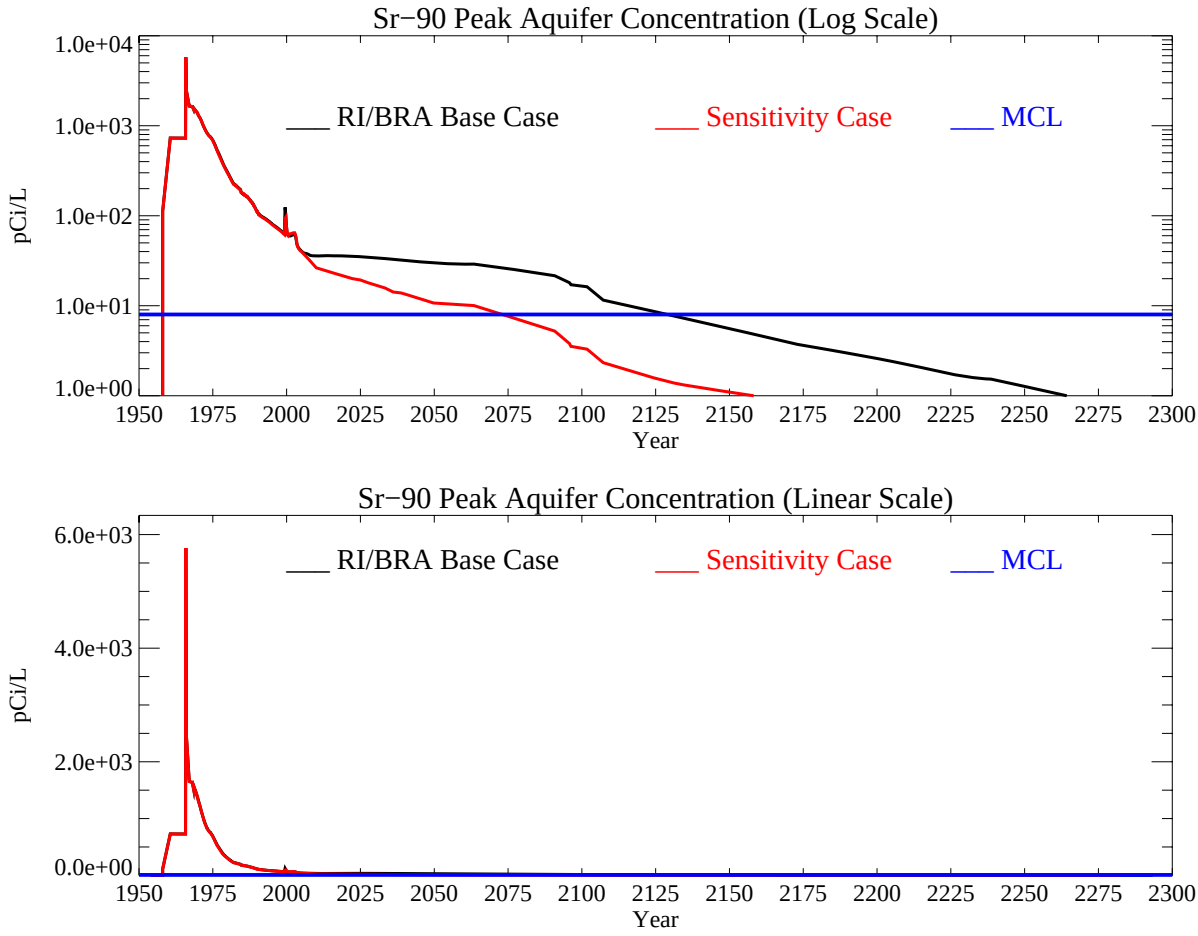

Figure J-11-70. Sr-90 peak aquifer concentrations with increased dispersivity (pCi/L) The MCL is shown in blue, the RI/BRA model in black, and this sensitivity run in red.

J-11.7 Summary of Sensitivity to Hydrologic Parameters

Under the hydrologic conditions examined in this sensitivity analysis, the geochemical processes observed in the one-dimensional model were preserved. We saw that in all cases, a fraction of the strontium moves relatively rapidly through the alluvium either complexed with nitrate ion, or because of inhibition of adsorption as a result of competition with elevated sodium and calcium concentrations in solution. The relative abundance of sodium and calcium are influenced by the saturation initially in the pore space of the alluvium and by the recharge rates through the alluvium. Once the sodium-bearing waste peak has passed through the alluvium, the remaining strontium on the ion exchange sites is released much more slowly. Within the parameters spanned here, the sodium-bearing waste pulse leaves the alluvium between 5 and 10 years after release (Table J-11-1).

In the RI/BRA base case, assuming an infiltration rate of 18 cm/yr, 12,336 Ci of Sr-90 were released within the first 10 years. In the case where the infiltration rate was increased to 39 cm/yr the HCO_3 became more abundant. This buffers the pH, reducing the amount of Sr-90 contained in the initial fast release from the alluvium. Increasing the infiltration rate dilutes the raffinate, resulting in less competition and complexing. Decreasing the infiltration rate increases the aqueous phase Sr^+ ion, which increases the amount of Sr-90 in that initial release, but it takes a little longer. Over the range of infiltration and wetting conditions representative of the tank farm liner and alluvium properties, there was considerable sensitivity in the amount of Sr-90 predicted to leave the alluvium within the first 10 years. At a low infiltration rate of 3 cm/yr, the Sr-90 leaving the alluvium at 10 years was predicted to be 7,243 Ci, while at 18 cm/yr and 39 cm/yr, the first released activity was 12,272 Ci and 5,536 Ci, respectively. This 6,736 Ci range produced a remarkably small difference in predicted 2095 peak aquifer concentrations. The relative insensitivity of aquifer concentrations to a seemingly large change in activity leaving the alluvium is due to the coupled hydrogeochemical processes, and is dominated by the fact that the Sr-90 arriving in the aquifer is transported via dispersion as opposed to pure advection.

This system is very sensitive to large changes in infiltration rate that result when it is assumed most of the anthropogenic water is released in northern INTEC. If the infiltration rate is on the order of 116 cm/yr in the regions outside of the tank farm, the six fold increase in infiltration rate increases peak aquifer concentrations by a factor of 18.4 Relatively large increases in infiltration rates produce higher saturations in the upper shallow and upper deep interbeds underlying northern INTEC. This increased the lateral spreading of contaminants, and also increases the vertical velocities. The 116 cm/yr corresponded to 52 million gallons/yr added to an infiltration rate from precipitation of 18 cm/yr. For comparison, the Big Lost River contributes on the order of 1.9 m/yr per meter of river length and its influence is apparent in all of the time-history plots of peak aquifer concentration. Although Sr-90 concentrations at INTEC are sensitive to high flux rates, removing a distributed water source had very little effect on predicted concentrations. When the anthropogenic water was assumed to be distributed throughout INTEC, stopping the water losses in year 2035 decreased concentrations in year 2095 by only 35%. The relatively small gain resulting in this case is attributable to the large difference between anthropogenic water losses and infiltration from precipitation. If it is assumed that the anthropogenic water is distributed throughout INTEC, as opposed to being focused in northern INTEC, precipitation is the dominant source of infiltration.

Predicted Sr-90 concentrations are sensitive to the assumed land-use scenario. If the production wells (CPP-1 and CPP-2) are removed from the influence of INTEC natural attenuation in central INTEC increases. At the same time concentrations are predicted to increase in northern INTEC. Increases occur in northern INTEC because when the production wells are in use the two production wells increase dispersion. There is some evidence that the two production wells also remove contaminants from the aquifer as a result of pumping. Contaminant sampling supports the latter observation (ICP 2004), and the relatively flat head gradient in central INTEC supports the former observation. Although predicted concentrations are sensitive to the presence of the production wells, they are not sensitive to their time of removal. The insensitivity is caused by continued arrival of Sr-90 from the vadose zone being larger than the natural attenuation processes in the aquifer.

Table J-11-1. Hydrologic parametric sensitivity summary. All Sr-90 activities are undecayed.

	Infiltration Rate (cm/yr)			Anthropogenic Water					Dispersivity
	I=39	**I=18**	**I=3**	**Focused in Northern INTEC**	**Losses Stopped in 2035**	**Pumping Stopped in 2012**	**Pumping Stopped in 2035**	**Pumping Stopped in 2096**	**10% of domain**
Alluvium Statistics									
Years after CPP-31	**Activity Leaving Alluvium (Ci)**								
5 yrs	1575	5187	1342	5187	5187	5187	5187	5187	5187
10 yrs	5536	12272	7243	12272	12272	12272	12272	12272	12272
15 yrs	5558	12310	7845	12310	12310	12310	12310	12310	12310
20 yrs	5580	12336	8037	12336	12336	12336	12336	12336	12336
Activity Remaining in Alluvium (Ci)	10320	3564	7863	3564	3564	3564	3564	3564	3564
Effective K_d (mL/g) at 20 years	13	2	6.4	2	2	2	2	2	2
Vadose Zone Statistics									
Peak Concentration (pCi/L)	3.0E9	2.0E9	1.9E9	4.0E8	2.0E9	2.0E9	2.0E9	2.0E9	7.3E8
Year Peaked	1979	1979	1978	1978	1978	1978	1978	1978	1978
Aquifer Statistics									
Peak Concentration (pCi/L) in 2095	27.3	18.6	8.9	343.0	12.0	11.9	11.9	18.6	4.0
Year C is below 8 pCi/L	2148	2129	2099	2214	2121	2108	2107	2108	2074

shaded cells = RI/BRA base case

J-12 VADOSE ZONE AND AQUIFER CALIBRATION

This section presents the aquifer and vadose zone calibration results. As observed in the RI/BRA simulations, the impact of varying the geochemical and hydrologic parameters on aquifer calibration is minimal. This insensitivity is due to the fact that Sr-90 in the SRPA prior to year 1990 is largely a result of the injection well (CPP-03), and its failure. The relatively small amount of Sr-90 arriving in the aquifer prior to 2005 (where we have field data) from land surface sources does not influence aquifer calibration. On the other hand, calibration to perched water is sensitive to the hydrogeochemical parameterization in both the alluvium and interbeds. The calibration to observed Sr-90 in aquifer wells is presented first, followed by the detailed discussion of vadose zone perched water calibration.

J-12.1 Aquifer Calibration Results

The primary source of Sr-90 was associated with the tank farm releases, with 18,100 Ci released in the tank farm, and 24.3 Ci discharged in the CPP-03 injection well. Field observations of Sr-90 in the aquifer are a direct result of the CPP-03 injection. Because of the retardation of Sr-90 in the vadose zone, most of the Sr-90 released in the tank farm will never reach the aquifer. The amount that has been predicted to reach the aquifer from surface sources is on the order of 1% of the amount injected in CPP-3. The disposal history for Sr-90 in the CPP-3 injection well is fairly complete as illustrated in Figure J-12-1. The raw data (Figure J-12-1 top) for releases were smoothed (Figure J-12-1 bottom) using an averaging process to facilitate incorporation into the numerical model.

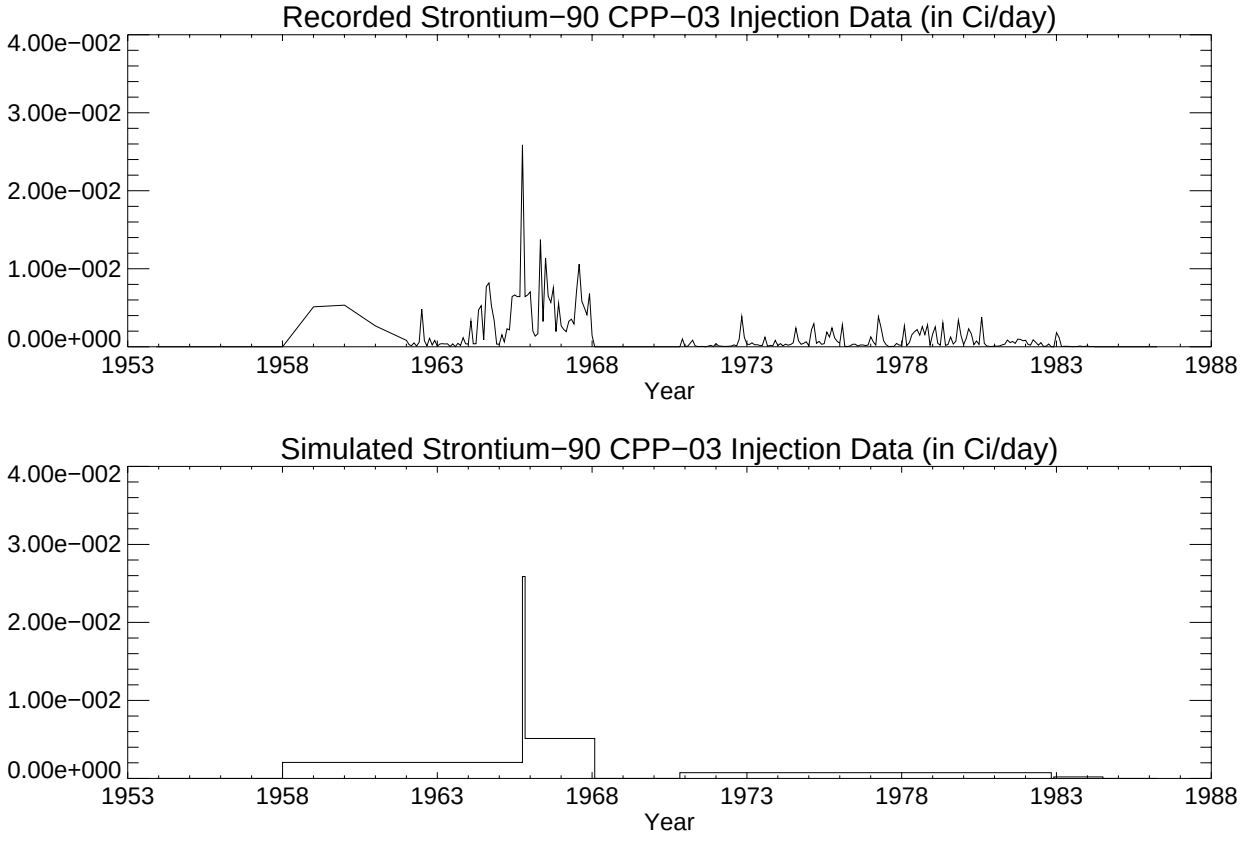

Figure J-12-1. Reported (top) and simulated (bottom) strontium-90 disposal in CPP-03 (Ci/day).

Matching the Sr-90 concentration history in the aquifer required adjusting the sorption coefficients in the aquifer materials. The best match between the arrival of discernible peaks and their concentrations were obtained by using a retardation factor of 4 for the basalt, corresponding to a K_d of 0.035 mL/g, and an H-I interbed K_d of 22 mL/g (from Appendix D).

Within the aquifer, Sr-90 has been monitored more frequently than contaminants with the exception of tritium. This data indicates that Sr-90 had traveled south as far as USGS-112 in the late 1980s. Predicted aquifer concentrations matching the southern extent are shown in Figure J-12-2. The model results shown in Figure J-12-2, are a simplification of the 3-dimensional concentrations predicted for the aquifer. To represent higher dimensional results in plan view, we have chosen the highest 15 m average concentration at any planar coordinate. This depth interval does not, in general, correspond to any particular well screen location, but does represent the highest pumpable concentration.

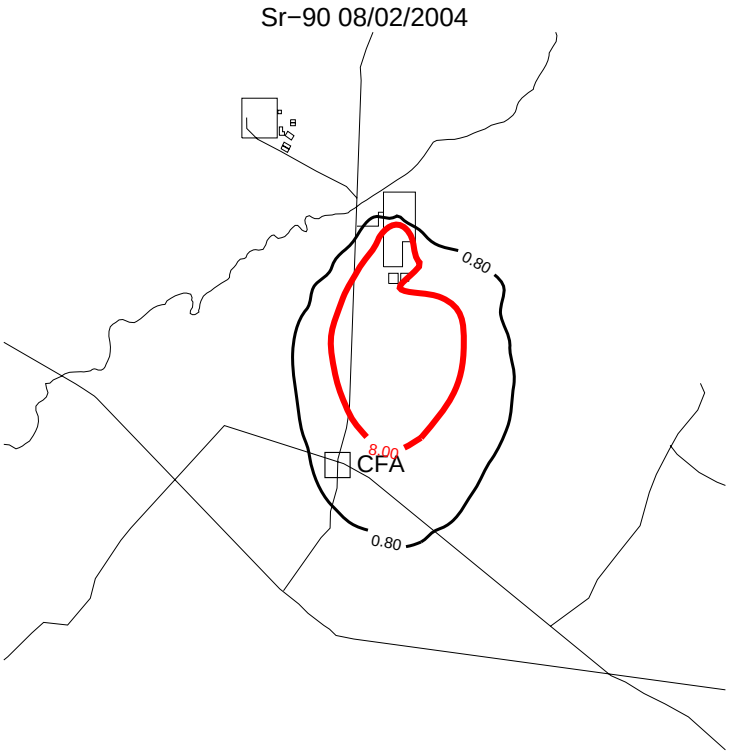

(a)

Figure J-12-2. Maximum simulated Sr-90 concentrations (pCi/L) on the base grid averaged over a 15m well screen in 2004 for the RI./BRA base case.

A 15 m well screen was chosen to represent peak concentrations throughout this analysis to account for real pumping effects. Concentrations representing the average are fairly insensitive to the assumed screened length prior to the arrival of Sr-90 in significant quantities from the vadose zone. This is largely due to Sr-90 currently in the aquifer being injected through a very large screened interval. The large screened interval distributes Sr-90 relatively uniformly over the vertical as shown in Figure J-12-3 for the ICPP-179x series wells located between the INTEC and the CFA. As shown by the 2003 data (asterisks) the vertically distributed range is small, and as shown by the RI/BRA model results (solid line), the predicted concentrations are also fairly uniform over the vertical.

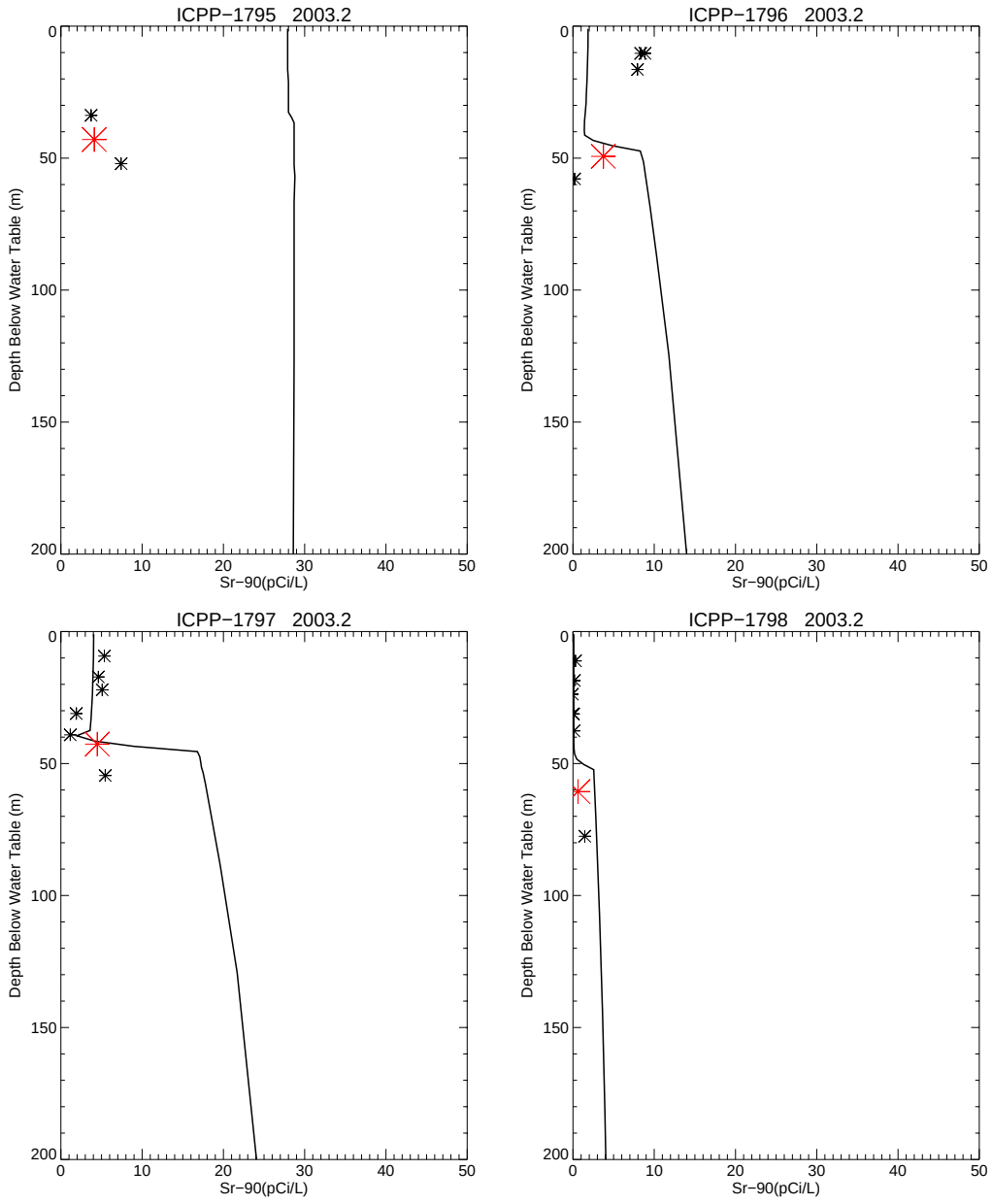

Figure J-12-3. Simulated and observed Sr-90 concentrations vs. depth in 2003 (simulated data using 15 m average=solid line, small asterisk=data taken in basalt, large red asterisk=data taken in the HI interbed, pCi/L).

Concentration histories for aquifer wells are given in Figures J-12-4 through J-12-8. A well -by-well comparison shows that although sampling was extensive, there are a large number of wells in which data collection did not begin until the mid 1980's. The presentation of these wells is sorted by distance from the CPP-03 with wells nearer CPP-03 presented first and wells closer to CFA presented last. The simulated concentrations plotted on these figures corresponds to the RI/BRA model.

In general, the timing and magnitude of predicted Sr-90 concentrations match the further wells quite well. On the other hand, the predicted arrival of peak concentrations in wells closer to INTEC occurs earlier than observed in the data, and predicted concentrations are too high. This disparity suggests that either there are two regions of velocity or there are two distinct regions of adsorption occurring in the aquifer. It is likely that a combination of both occurs, and that the combination is a function of the chemistry of the fluids injected with the Sr-90. The aquifer model assumes a uniform K_d throughout the aquifer domain, and does not account for potential changes in water chemistry as the injectate migrates down gradient from the injection well. It is possible that, like in the vadose zone, there are gradations in retardation in the aquifer as the sodium bearing injectate is diluted.

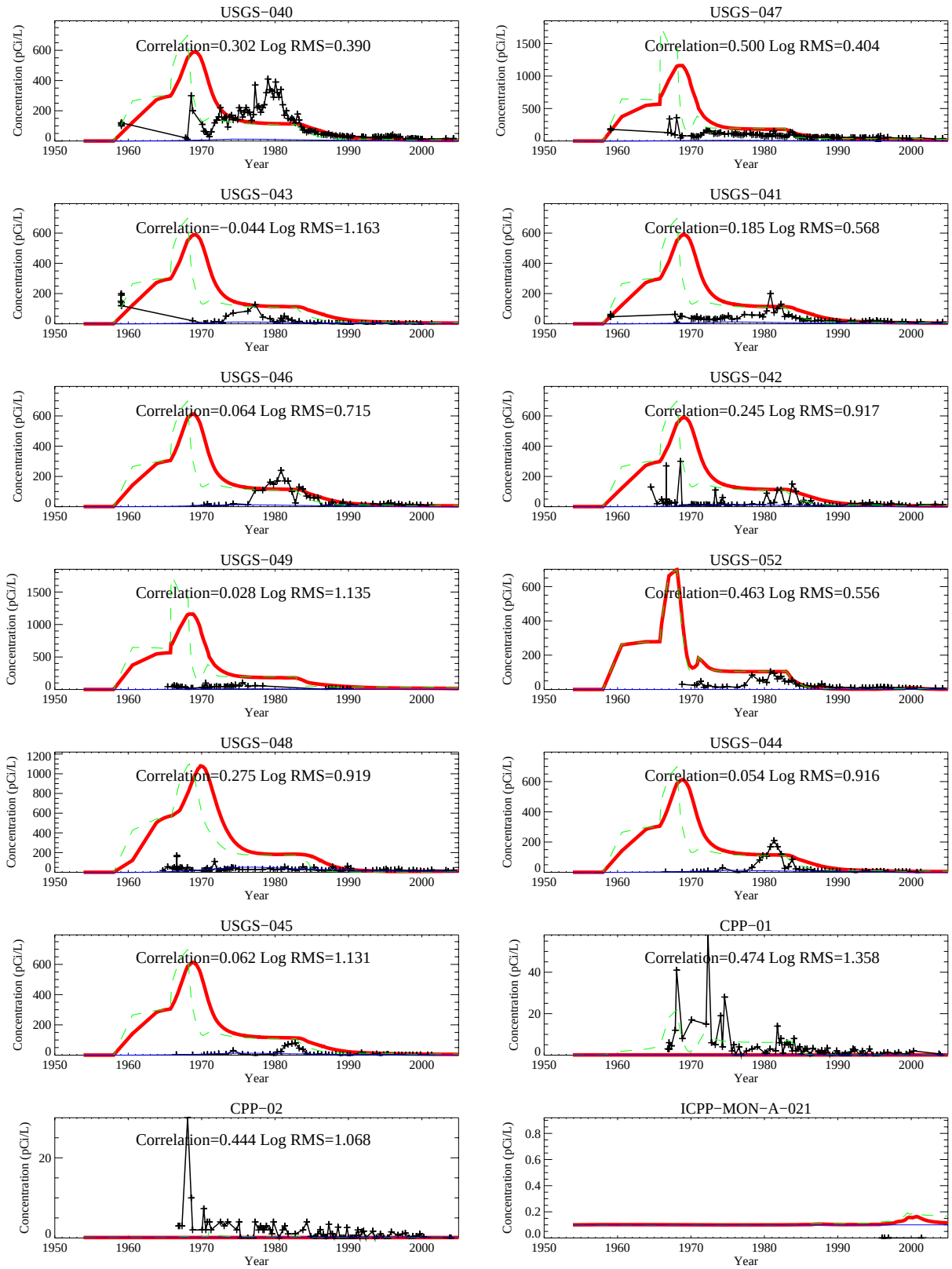

Figure J-12-4. Simulated and observed Sr-90 concentration histories (pCi/L) (measured=black crosses, thick red=model at screen center, dashed green=model top, blue=model bottom).

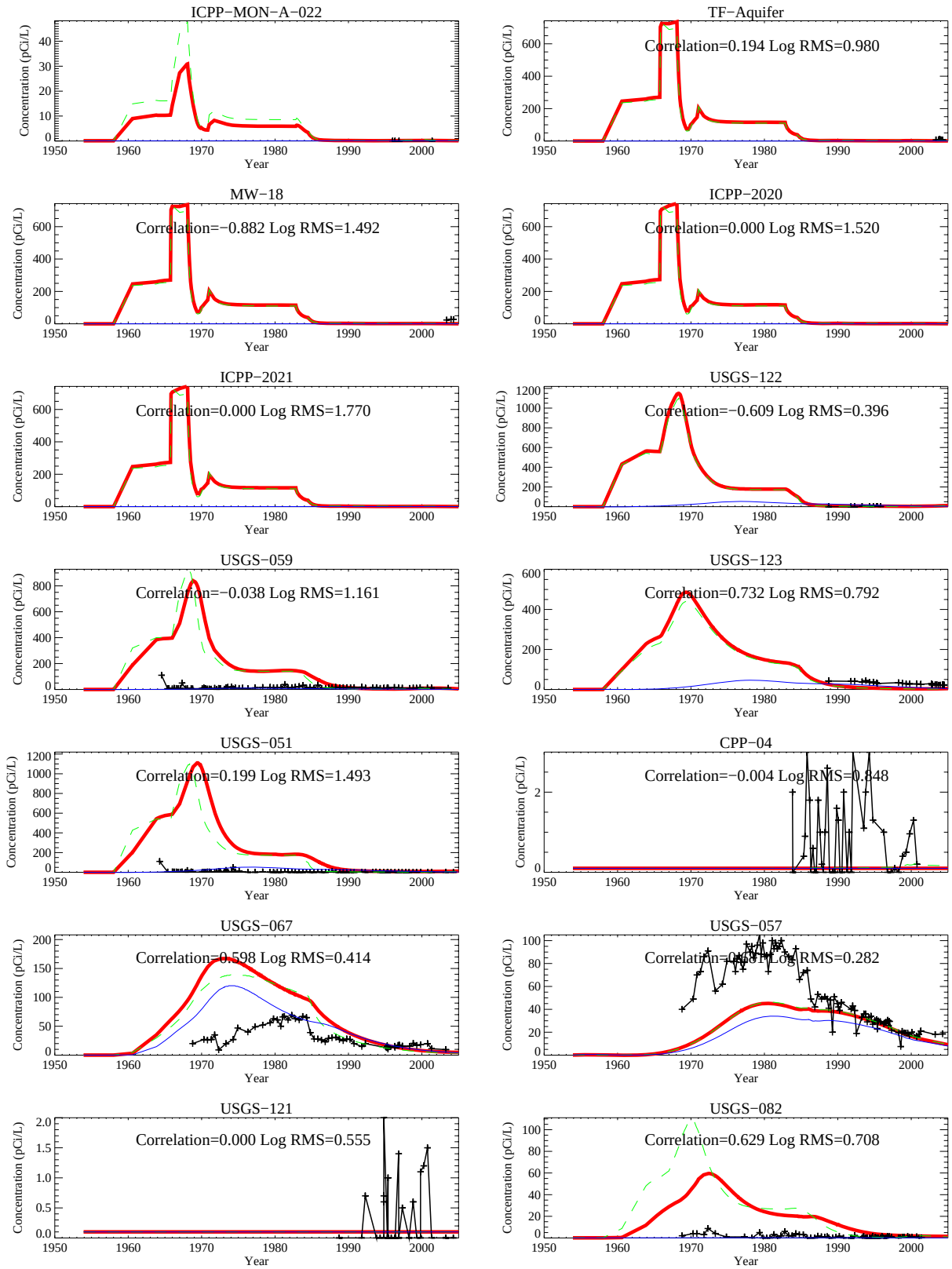

Figure J-12-5. Simulated and observed Sr-90 concentration histories (pCi/L) (measured=black crosses, thick red=model at screen center, dashed green=model top, blue=model bottom).

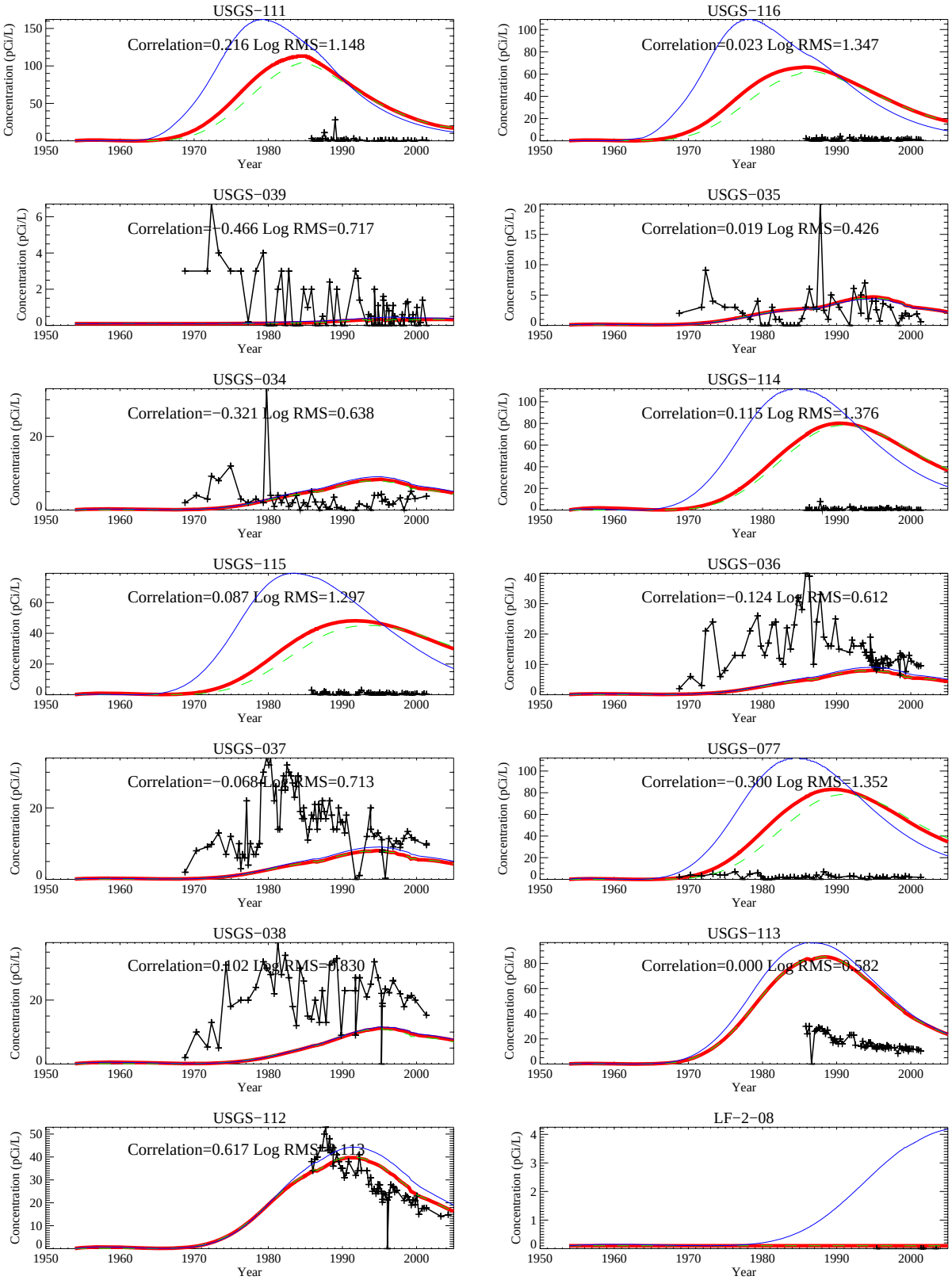

Figure J-12-6. Simulated and observed Sr-90 concentration histories (pCi/L) (measured=black crosses, thick red=model at screen center, dashed green=model top, blue=model bottom).

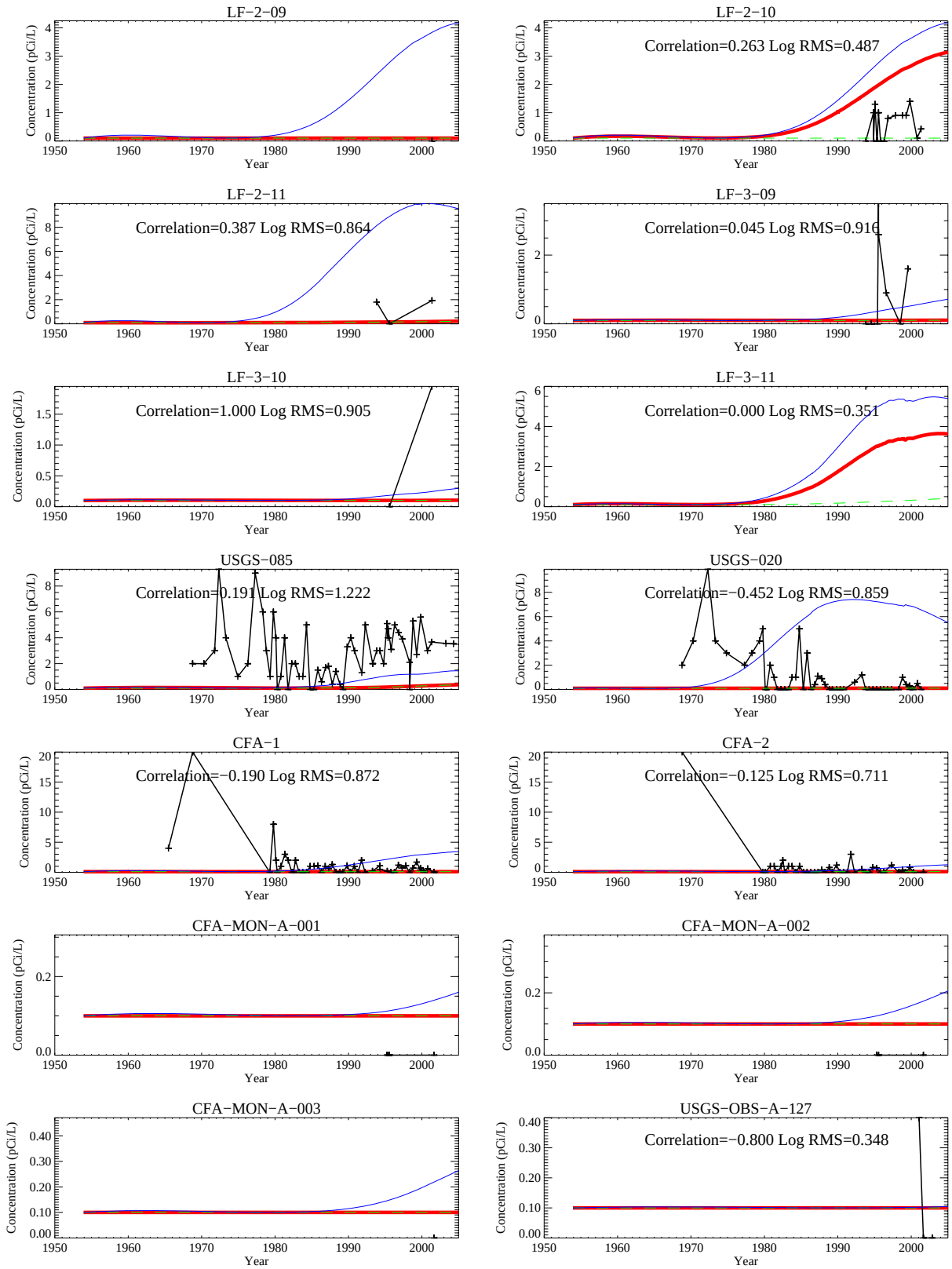

Figure J-12-7. Simulated and observed Sr-90 concentration histories (pCi/L) (measured=black crosses, thick red=model at screen center, dashed green=model top, blue=model bottom).

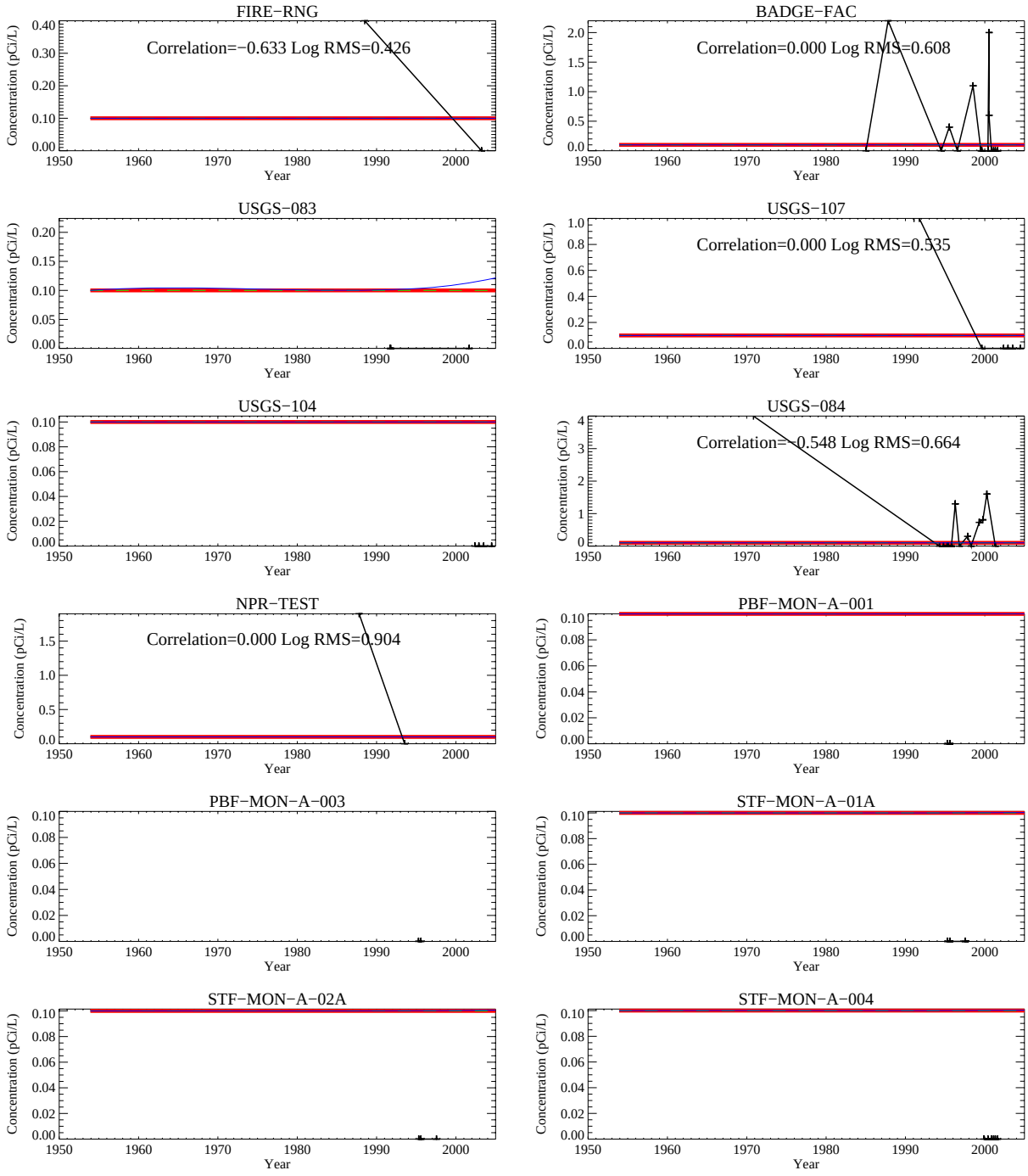

Figure J-12-8. Simulated and observed Sr-90 concentration histories (pCi/L) (measured=black crosses, thick red=model at screen center, dashed green=model top, blue=model bottom).

J-12.2 Vadose Zone Calibration Results For The RI/BRA MODEL

There are five primary regions of perched water that are considered in vadose zone calibration. These are the 1) northern upper shallow, 2) northern lower shallow, 3) northern deep, 4) southern shallow, and 5) southern deep perched waters. Each of these is influenced differently by the sources of Sr-90 contributing to their contamination, and by the hydrogeochemical parameters used in the model. The effect of model parameterization is discussed for each zone below.

J-12.2.1 Northern Upper Shallow Perched Water Sr-90

Data for the upper shallow perched water wells is presented in Figure J-12-9. In general, the data were collected well after Sr-90 initially arrived in this water body, and in many wells, the data only captures a small segment of the contaminated period. In only one well is a relatively complete concentration history available. This better data set was obtained for the CPP-55-06 well, where concentrations were fairly high.The key points to note in the available data include:

- High concentrations (above 10,000 pCi/L) have been observed in CPP-33-1, MW-5-2, MW-2, and MW-4-2. These wells are close to the tank farm with the exception of MW-5-2 which is further west and south. The highest concentration (458,000 pCi/L) was observed in 2004 in CPP-33-1, but only one data point is available in that well. Concentrations in MW-5-2 were near 100,000 pCi/L during the 1993-1995 time period, but have been below 20,000 pCi/L since 2001. Concentrations in Well MW-2 have followed a similar pattern to those in Well MW-5-2 and were measured at 514,000 pCi/L in 1993 and at 160,000 pCi/L in 2004. Sr-90 in Well MW-4-2 is also high and was measured at 5,800 and 11,900 pCi/L in 1993 and 1995, respectively.
- The other northern upper shallow perched water Sr-90 concentrations have been near or below 10 pCi/L except one measurement at well MW-6 in 2004 at 8,100 pCi/L. The previous observations dating back to 1993 were near 10 pCi/L.

The Sr-90 concentrations in the upper shallow perched water may be declining and peak concentrations in many of these wells may have occurred prior to 1995. Sr-90 concentrations in this region are declining more rapidly than would be predicted by radioactive decay alone, suggesting an active advective or dispersive flow component. Based on one measurement, concentrations in CPP-33-1 might be an exception.

The RI/BRA model predicted (red line) and observed (blue asterisk and line) Sr-90 concentrations for the northern upper shallow perched water wells are illustrated in Figure J-12-9. In general, the model agrees with the observed patterns of Sr-90 concentrations, but it tends to over predict the values observed in wells north and west of the tank farm, but under predicts the values south and east of the tank farm. It predicts that the highest simulated concentrations occur beneath the tank farm and immediately south and east of the tank farm. Overpredicting concentrations suggests that the model is overestimating north and west lateral water movement within and above the first interbed and underestimating lateral movement to the south and east.

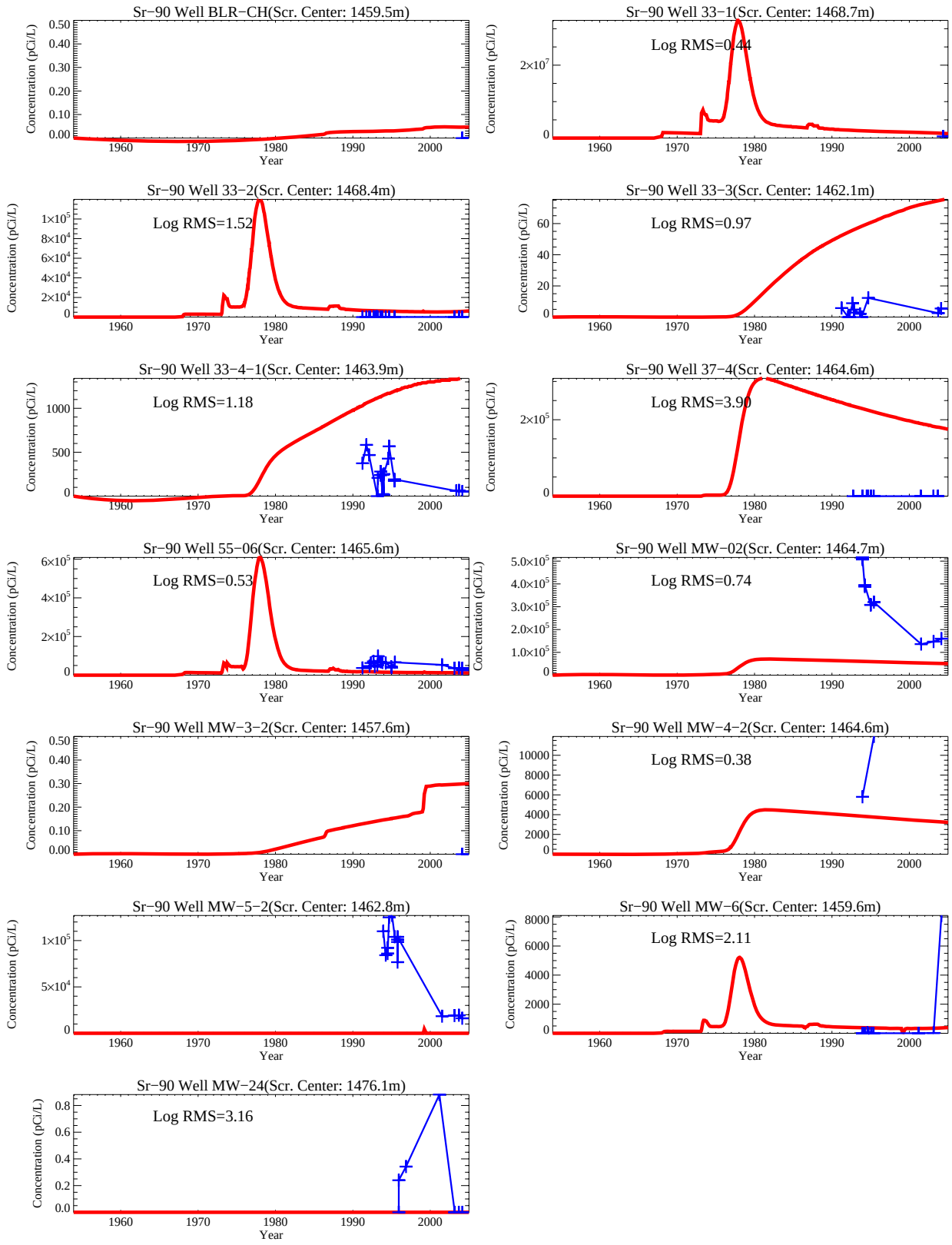

Figure J-12-9. Comparison of model predictions to field data for Sr-90 in the northern upper shallow perched water (red = predicted, blue = field data).

J-12.2.2 Northern Lower Shallow Perched Water Sr-90

In Figure J-12-10, data for wells in the northern lower shallow perched water are shown in blue. These figures show that wells within this region have not provided sufficient concentration-time data to assess whether the peak concentrations have been reached. Declining Sr-90 concentrations observed in the northern upper shallow perched water would suggest that the northern lower shallow perched water concentrations should be increasing -- reflecting the arrival of Sr-90 from the upper region. Available data in this lower region is sparse, and overall interpretation is uncertain. The key observations include:

- Declining concentrations have been observed in MW-20-2. The highest concentration (25,800 pCi/L) in this region was found in this well in 1995 has fallen to 21,224 pCi/L as of 2004.
- The concentration history in MW-10-2 is highly variable. Measured concentrations have ranged from 17,200 pCi/L in 1995, zero in 2001, and were back to 16,900 in 2004.
- Observed concentrations in the TF-SP and BLR-SP were near zero, but few measurements are available.

The spatial distribution of Sr-90 in the northern lower shallow perched water Figure J-12-10 is similar to that in the northern upper shallow perched water, and this distribution is reflected in the model predictions (red line). The highest simulated concentrations were predicted to be beneath the tank farm and immediately south and east of the tank farm. Like the upper region, simulated concentrations in this lower region were mostly higher than the observed concentrations. The large abrupt changes in concentrations predicted to occur in this region are due to the quarterly step change in the simulated Big Lost River recharge. The model predicts the 140-ft interbed is affected by the river to a greater extent than is the 110-ft interbed (see Appendix A, Section 6.2.2)

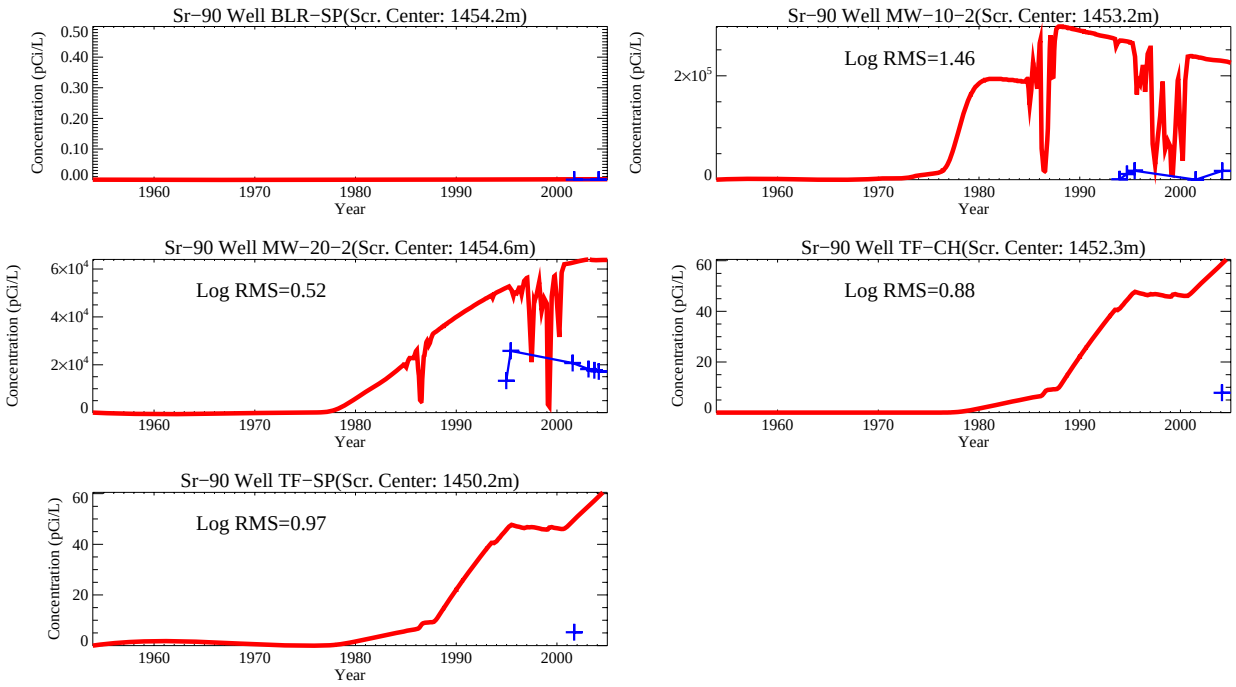

Figure J-12-10. Comparison of model predictions to field data for Sr-90 in the northern lower shallow perched water (red = predicted, blue = field data).

J-12.2.3 Northern Deep Perched Water Sr-90

Data for the wells completed in the northern deep perched water are shown in blue in Figure J-12-11. The Sr-90 retardation in the interbeds and the depth of the northern deep perched water make the tank farm an unlikely source of the Sr-90 in this region. The Sr-90 found in the northern deep perched water was most likely a result of the CPP-03 injection well failure. The highest observed Sr-90 concentrations found in this region coincide with the CPP-3 injection well repair date and the peak concentrations were close to the service waste water concentrations.

The highest observed Sr-90 concentrations (2,500 pCi/L) in this region were found in Well USGS-50 in 1970. The worst match in this water body occurred at well USGS-050, where concentrations are overpredicted by a factor of 400 ($380=10^{2.58}$). As discussed in Appendix A, Section ,6.3.2.1 the casing in this well has historically allowed downward migration of contaminants from higher elevations. The highest concentrations in the vadose zone pore water occur in the shallow interbeds with lowest concentrations appearing deeper. By allowing rapid migration through this well, the pore water near USGS-050 has much higher concentrations than observed in other deep wells. This leakage has not been accounted for in any of the vadose zone simulations presented here. In most of the key perched water wells, the difference between predicted and observed concentrations differs by less than a factor of 5 (log RMS< 0.76), which is very good given the overall complexity of the vadose zone at INL

The peak observed Sr-90 concentration in Well MW-18-1 was 207 pCi/L in 1995, and is most likely a reflection of the CPP-3 injection well because of the similarity to observed USGS-50 concentrations. Unlike predictions for the USGS-50 well, the simulated concentrations in Well MW-18-1 are persisting and begin to increase during the 1980s. This difference occurs because the model predicts the CPP-3 injection well water moving eastward towards Well MW-18 to a greater extent than northward towards Well USGS-50. The field data is inconclusive.

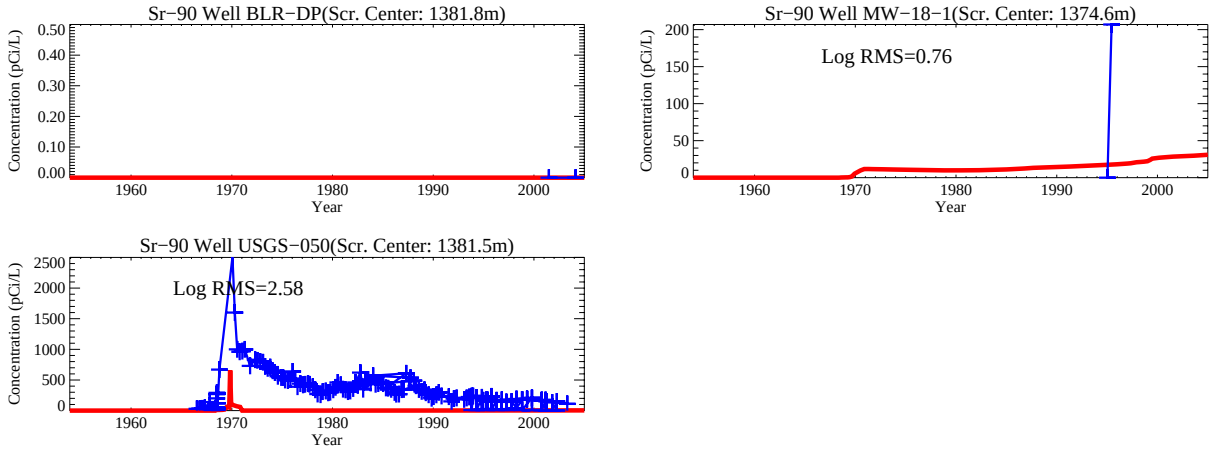

Figure J-12-11. Comparison of model predictions to field data for Sr-90 in the northern deep perched water (red = predicted, blue = field data).

J-12.2.4 Southern Shallow Perched Water Sr-90

Simulated (red) and observed (blue) Sr-90 concentration histories in the southern shallow perched water are illustrated in Figure J-12-12. This water body is associated with the 110-ft and 140-ft interbeds. Primary sources of Sr-90 in this region are the CPP-02 abandoned french drain and the former percolation ponds. The CPP-02 abandoned french drain operated from 1954 through 1966, received 4.78E7 gallons of water and 33.8 Ci of Sr-90. The percolation ponds operated from 1984-2002 and received service waste until the LET&D facility became operational in 1993. High concentrations in this region have been observed in MW-15 with much lower concentrations observed in other wells.

The highest Sr-90 concentrations were observed in Well MW-15 (22,100 pCi/L) in 1995, and high concentrations have been observed since its installation in 1994. This well is located near the southeast corner of CPP-603, and near site CPP-02. Concentrations at this location are too high to have originated in either the former percolation ponds, or the OU 3-13 Group-3 soil sites. For many years it has been known that elevated Sr-90 activities are present in the alluvium and shallow perched water near the CPP-603 spent fuel storage basins. Sections 2.2.6.1.1 and 2.3.2.2 of the OU 3-13 Work Plan (INEL, 1995) include detailed discussions of historical radionuclide concentrations in this area, and based on the low chloride concentrations, contaminated perched water in MW-15 is not believed to be derived from the former percolation ponds. Rather, the presence of Sr-90 and other fission products in the shallow perched water at this location is attributed primarily to historical releases of contaminated water from the spent fuel storage pools, including CPP-02 (Robertson et al. 1974).

Most of the observed data in the southern shallow perched water begins in the mid 1980s when the PW series wells were installed. A well defined concentration history is observable in this well series with first arrival coinciding with the percolation pond start up. The percolation ponds were excavated to basalt leaving sediments in topographical lows during their construction. The model placed the percolation pond water in the alluvium grid block immediately above the basalt, requiring injectate to migrate through the half-grid block of alluvium prior to entering the underlying basalt. The RI/BRA model used an alluvium K_d of 2 mL/g and an interbed K_d of 22 mL/g, which allows close approximation to wells PW-4, PW-5, and PW-2. The relatively low K_d allows migration from CPP-02 to arrive early in well PW-1, but by year 1990 concentrations are very close to measured values as shown by the RMS of 0.42 in that well. If anything, the simulated concentrations near the percolation pond is slightly delayed and of lower amplitude than observed in the data. The sodium concentration in the percolation pond water resulting from the INTEC water softening may have lowered the effective alluvium and interbed K_ds near the former percolation ponds below these assumed values. Concentrations of both Sr-90 and H-3 observed in Well PW-6 indicate percolation pond water reached this well. However, the model did not predict substantial amounts of percolation pond water arriving at this location.

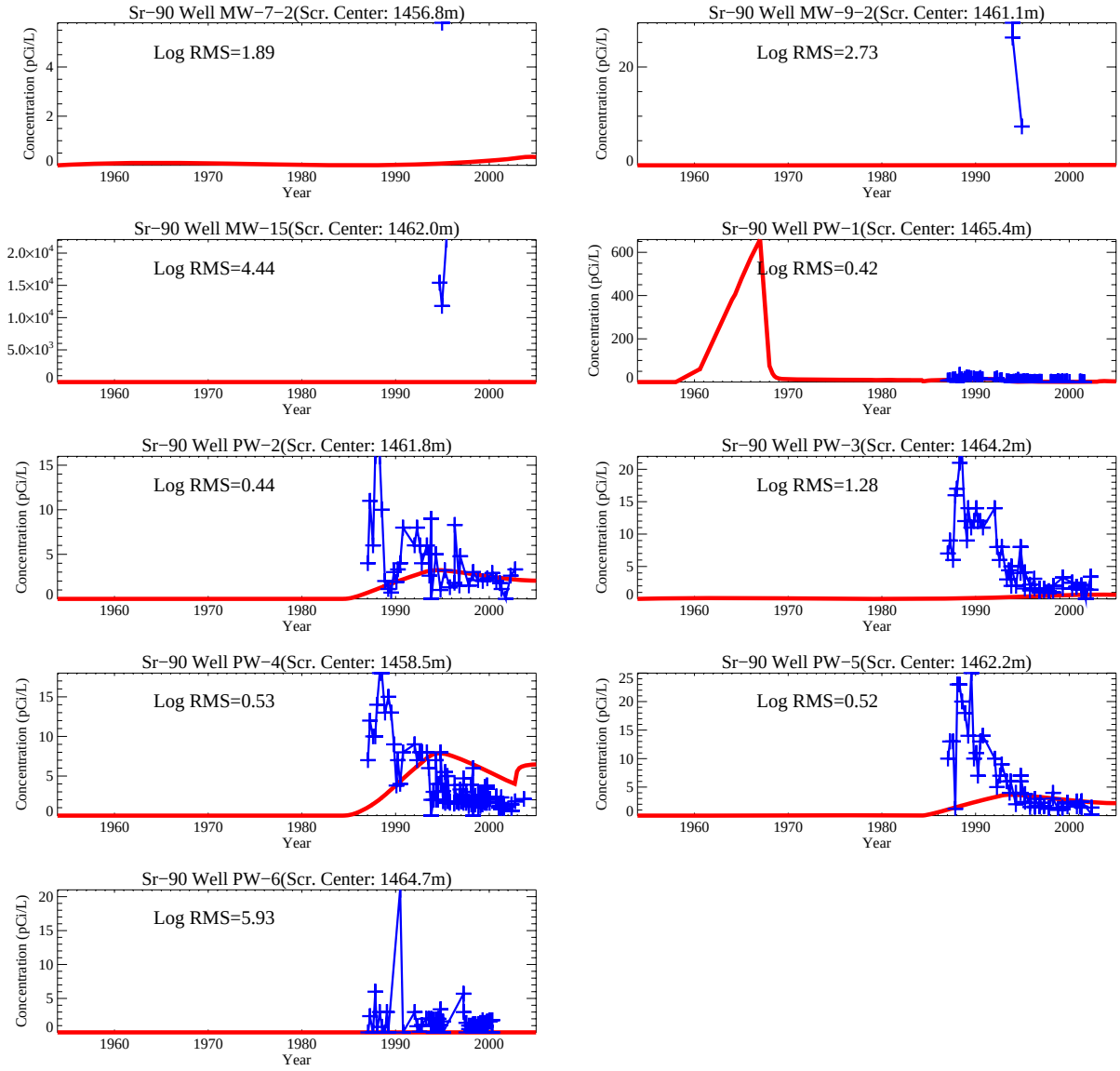

Figure J-12-12. Comparison of model predictions to field data for Sr-90 in the southern shallow perched water (red = predicted, blue = field data).

J-12.2.5 Southern Deep Perched Water Sr-90

The simulated and observed Sr-90 concentrations in the southern deep perched water wells is illustrated in Figure J-12-13 by the red and blue lines, respectively. The southern deep perched water is associated with the 380-ft interbed, but perched water has been encountered higher than 380-ft. As with the southern shallow perched water, the Sr-90s contamination sources are the CPP-02 abandoned french drain, the OU 3-13 group 3 soil sites and the service waste discharged into the former percolation ponds. Wells MW-1-4 and CS-CH lie near the northern most extent of the southern well grouping area and they most likely see contamination resulting from the CPP-3 injection well, OU 3-13 Group 5 soil sources, and possibly the tank farm releases.

The highest observed Sr-90 concentration in the southern deep perched water was found in Well 1804M at 16.9 pCi/L in 2002. Observed concentrations were 5.2 pCi/L in MW-1-4 at 5.2 pCi/L in 1994, 2.2 pCi/L in MW-17-2, and 1.1 pCi/L in well 1807L in 2002. Predicted concentrations using the RI/BRA model are quite close to these values in all but 1807L and MW-1-4 as indicated by the log RMS.

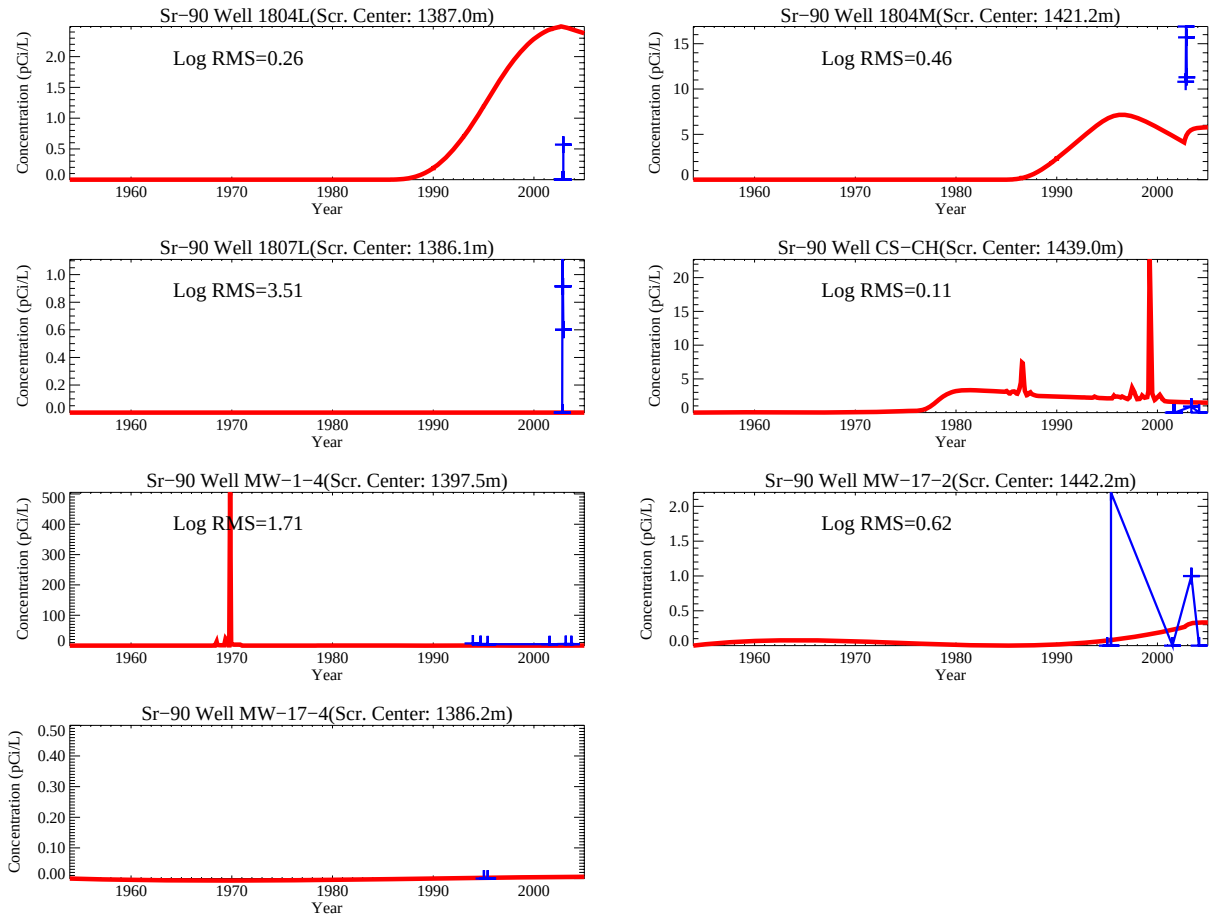

Figure J-12-13. Comparison of model predictions to field data for Sr-90 in the southern deep perched water (red = predicted, blue = field data).

J-12.3 Sensitivity of Perched Water Calibration to Hydrogeochemical Parameters

The log10 root mean square error for each of the sensitivity runs is summarized in Tables J-12-1 through J-12-10. The results are presented separately for each perched water zone, starting with the northern upper shallow perched water. In the discussion of each perched water body, there are two tables. In the first table, the minimum, average, and maximum log10 RMS is given with an indicator denoting the best match to field data and the figure in the body of the report in which the comparison to field data can be found. The second table contains the log10 RMS for each well used to derive the statistics in the first table. It is included to explain why the best match to field data does not always correspond to the smallest average log10 RMS error. The differences are largely related to the absolute maximum of observed field data. Even though the average error for a given simulation might be smaller, the average can be biased by wells in which the concentration is low. Prediction of long-term risk is driven by the highest concentrations, and the noted best match to field data takes this difference into account qualitatively.

J-12.3.1 Summary of Northern Upper Shallow Perched Water Calibration

The average log10 RMS (Table J-12-1) in the northern upper shallow perched water ranges from 1.04 to 1.50. In general, the lower mismatch errors were associated with the sensitivity run in which a CEC of 7 meq/100 g and interbed K_d of 50 mL/g were used. This parameter set probably overestimates the CEC, which is more likely in the 2-3 meq/100 g range. Decreasing the CEC increases the average log10 RMS because it results in overpredicting concentrations in wells far from CPP-31. Using only the highest concentration wells (MW 33-1, MW 33-2, 55-06, and MW-02), the lowest log10 RMS is obtained with more anthropogenic water in northern INTEC (Table J-12-2). As explained in Section J-11.3, the better match in this case occurs because more water allows flow above the 110-ft interbed.

Table J-12-1. Northern upper shallow perched water calibration summary.

Simulation	Minimum Log10 RMS	Average Log10 RMS	Maximum Log10 RMS	Figure #
RI/BRA Model: Alluvial CEC=2 meq/100 g, Interbed K_d=50 mL/g	0.38	1.33	3.90	J-8-14
Geochemical Parameter Sensitivity				
Alluvial CEC of 3 meq/100 g, Interbed K_d=50 mL/g	0.40	1.34	3.84	J-10-6
Alluvial CEC of 7 meq/100 g, Interbed K_d=50 mL/g	0.24	1.04	3.62	J-10-21
Alluvial CEC of 2 meq/100 g, Interbed K_d=22 mL/g	0.16	1.49	4.21	J-10-32
Alluvial CEC of 2 meq/100 g, Interbed K_d=78 mL/g	0.15	1.26	3.72	J-10-43
Hydrologic Parameter Sensitivity				
Lower 3 cm/yr Infiltration through the tank farm Liner	0.25	1.18	3.92	J-11-6
Higher 39 cm/yr Infiltration through the tank farm Liner	0.34	1.33	3.89	J-11-18
Anthropogenic Water Losses Focused in Northern INTEC	0.16	1.34	4.11	J-11-29
Anthropogenic Water Losses Stopped in 2035	0.38	1.33	3.90	J-11-40
Larger Interbed Dispersivity	0.20	1.50	2.80	J-11-64

.

Table J-12-2. Northern upper shallow perched water calibration by well and simulation

Simulation	Well Name										
	33-1	**33-2**	**33-3**	**33-4-1**	**37-4**	**55-06**	**MW-02**	**MW-4-2**	**MW-20-2**	**MW-24**	**MW-5-2**
RI/BRA Model: Alluvial CEC=2 meq/100 g, Interbed K_d=50 mL/g	0.4443	1.5244	0.9693	1.1809	3.8983	0.5346	0.7437	0.3771	0.5174	3.1556	0.0000
Geochemical Parameter Sensitivity											
Alluvial CEC = 3 meq/100 g	0.4013	1.4879	0.9165	1.1522	3.8428	0.4870	0.7896	0.4199	0.4663	3.4291	0.0000
Alluvial CEC = 7 meq/100 g	0.3752	1.4267	0.7197	0.9922	3.6192	0.4246	0.9608	0.5874	0.2417	0.0000	0.0000
Interbed K_d = 22 mL/g	0.4534	1.5582	1.5450	1.7933	4.2119	0.4299	0.4088	0.1619	1.1847	3.1550	0.0000
Interbed K_d =78 mL/g	0.4399	1.5149	0.6604	0.9078	3.7230	0.5410	0.9318	0.5574	0.1454	3.1583	0.0000
Hydrologic Parameter Sensitivity											
Tank Farm Liner Infiltration = 3 cm/yr	0.2760	1.4479	0.9620	1.1556	3.9179	0.7272	0.7695	0.4003	0.4349	2.6527	0.2501
Tank farm Liner Infiltration = 39 cm/yr	0.5458	1.7050	0.9641	1.1583	3.8928	0.3427	0.7093	0.3464	0.4895	3.1626	0.0000
Anthropogenic Water Losses Focused in Northern INTEC	0.1583	1.9068	1.5909	1.4150	4.1078	0.3177	0.2758	0.5902	0.8403	3.1026	0.3852
Anthropogenic Water Losses Stopped in 2035	0.4443	1.5244	0.9693	1.1809	3.8983	0.5346	0.7437	0.3771	0.5174	3.1556	0.0000
Larger Interbed Dispersivity	0.2332	1.5700	1.5447	1.4694	2.7967	1.5297	1.6295	1.7945	0.2017	1.9554	1.7920

J-12.3.2 Summary of Northern Lower Shallow Perched Water Calibration

The average log10 RMS in the northern lower shallow perched water (Table J-12-3) ranges from 0.91 to 2.02, for all simulations presented in this document. One of the better matches in this region was obtained with a larger dispersivity. As discussed in Section J-11.6, this is an artifact of weighting wells with lower concentrations equal to those with higher concentrations (Table J-12-4). As with the northern upper shallow perched water calibration, the second best match occurs with a slightly higher interbed K_d. In contrast with the northern upper shallow perched water calibration, increasing the anthropogenic water produced one of the worst matches. It is likely that there is more anthropogenic water being lost to infiltration than currently accounted for in the RI/BRA model. However, it is also likely that the interbed K_d is higher (closer to the 78 mL/g), and that not as much water as simulated in Section J-11.3 is lost to infiltration.

Table J-12-3. Northern lower shallow perched water calibration summary.

Simulation	Minimum Log10 RMS	Average Log10 RMS	Maximum Log10 RMS	Figure #
RI/BRA Model: Alluvial CEC=2 meq/100 g, Interbed K_d=50 mL/g	0.88	1.35	2.11	J-8-14
Geochemical Parameter Sensitivity				
Alluvial CEC of 3 meq/100 g, Interbed K_d=50 mL/g	0.83	1.31	2.08	J-10-6
Alluvial CEC of 7 meq/100 g, Interbed K_d=50 mL/g	0.64	1.16	2.00	J-10-21
Alluvial CEC of 2 meq/100 g, Interbed K_d=22 mL/g	1.55	1.79	2.23	J-10-32
Alluvial CEC of 2 meq/100 g, Interbed K_d=78 mL/g	0.51	1.12	2.06	J-10-43
Hydrologic Parameter Sensitivity				
Lower 3 cm/yr Infiltration through the tank farm Liner	0.86	1.36	2.17	J-11-6
Higher 39 cm/yr Infiltration through the tank farm Liner	0.90	1.40	2.22	J-11-18
Anthropogenic Water Losses Focused in Northern INTEC	1.48	2.02	3.33	J-11-29
Anthropogenic Water Losses Stopped in 2035	0.88	1.35	2.11	J-11-40
Larger Interbed Dispersivity	0.22	0.91	2.43	J-11-64

.

Table J-12-4. Northern lower shallow perched water calibration by well and simulation.

Simulation	Well Name			
	MW-6	MW-10-2	TF-CH	TF-SP
RI/BRA Model: Alluvial CEC=2 meq/100 g, Interbed K_d=50 mL/g	2.1067	1.4593	0.8763	0.9742
Geochemical Parameter Sensitivity				
Alluvial CEC = 3 meq/100 g	2.0776	1.4189	0.8256	0.9233
Alluvial CEC = 7 meq/100 g	1.9992	1.2741	0.6378	0.7302
Interbed K_d = 22 mL/g	2.2269	1.7527	1.5481	1.6271
Interbed K_d =78 mL/g	2.0646	1.3010	0.5079	0.6094
Hydrologic Parameter Sensitivity				
Tank farm Liner Infiltration = 3 cm/yr	2.1740	1.4367	0.8571	0.9574
Tank farm Liner Infiltration = 39 cm/yr	2.2190	1.4891	0.9021	0.9963
Anthropogenic Water Losses Focused in Northern INTEC	3.3289	1.4838	1.5915	1.6588
Anthropogenic Water Losses Stopped in 2035	2.1067	1.4593	0.8763	0.9742
Larger Interbed Dispersivity	2.4268	0.7489	0.2169	0.2455

J-12.3.3 Summary of Northern Deep Perched Water Calibration

The average log10 RMS in the northern deep perched water ranges from 1.1 to 1.96 (Table J-12-5 and J-12-6), for all simulations presented in this document. In general, the lowest mismatch errors were associated with the sensitivity run in which CEC=2 meq/100 g was used. In this specific case, the northern deep well that is really significant is USGS-050. In all cases, the peak concentration was under predicted in this well. As discussed above, this well was used as a temporary replacement injection well while CPP-03 was

repaired. Peak Sr-90 concentrations during the early 1970s were definitely introduced during the CPP-3 injection well failure, and the simulated and observed timing agrees. The measured concentrations in USGS-50 decline slowly after the 1970 repair period, where as the model predicts that concentrations would rapidly decrease after the repair. The continued high concentrations of Sr-90 in USGS-050 is attributed to leakage around the well casing that allows shallow high concentration perched water to directly enter the deep perched water zone.

Simulated concentrations in Well MW-18-1 are persisting and began to increase during the 1980s. This is because the model predicts that CPP-3 injection well water would move eastward towards Well MW-18 to a greater extent than northward towards Well USGS-50. The field data for well MW-18 is inconclusive.

Table J-12-5. Northern deep perched water calibration summary.

Simulation	Minimum Log10 RMS	Average Log10 RMS	Maximum Log10 RMS	Figure #
RI/BRA Model: Alluvial CEC=2 meq/100 g, Interbed K_d=50 mL/g	0.76	1.67	2.58	J-8-14
Geochemical Parameter Sensitivity				
Alluvial CEC of 3 meq/100 g, Interbed K_d=50 mL/g	0.78	1.70	2.63	J-10-6
Alluvial CEC of 7 meq/100 g, Interbed K_d=50 mL/g	0.85	1.87	2.88	J-10-21
Alluvial CEC of 2 meq/100 g, Interbed K_d=22 mL/g	0.09	1.10	2.11	J-10-32
Alluvial CEC of 2 meq/100 g, Interbed K_d=78 mL/g	1.09	1.96	2.84	J-10-43
Hydrologic Parameter Sensitivity				
Lower 3 cm/yr Infiltration through the tank farm Liner	0.77	1.67	2.57	J-11-6
Higher 39 cm/yr Infiltration through the tank farm Liner	0.75	1.66	2.57	J-11-18
Anthropogenic Water Losses Focused in Northern INTEC	0.07	1.13	2.20	J-11-29
Anthropogenic Water Losses Stopped in 2035	0.76	1.67	2.58	J-11-40
Larger Interbed Dispersivity	1.05	1.65	2.26	J-11-64

.

Table J-12-6. Northern deep perched water calibration by well and simulation.

Simulation	Well Name	
	MW-18-1	USGS-050
RI/BRA Model: Alluvial CEC=2 meq/100 g, Interbed K_d=50 mL/g	0.7558	2.5765
Geochemical Parameter Sensitivity		

Table J-12-6. Northern deep perched water calibration by well and simulation.

Simulation	Well Name	
	MW-18-1	USGS-050
Alluvial CEC = 3 meq/100 g	0.7774	2.6286
Alluvial CEC = 7 meq/100 g	0.8547	2.8755
Interbed K_d = 22 mL/g	0.0936	2.1101
Interbed K_d =78 mL/g	1.0893	2.8352
Hydrologic Parameter Sensitivity		
Tank farm Liner Infiltration = 3 cm/yr	0.7715	2.5691
Tank farm Liner Infiltration = 39 cm/yr	0.7489	2.5717
Anthropogenic Water Losses Focused in Northern INTEC	0.0678	2.1978
Anthropogenic Water Losses Stopped in 2035	0.7558	2.5765
Larger Interbed Dispersivity	1.0464	2.2624

J-12.3.4 Summary of Southern Shallow Perched Water Calibration

The average log10 RMS in the southern shallow perched water ranges from 0.85 to 3.04 (Table J-12-7) for all simulations presented in this document. Not considering the magnitude of observed concentrations, the lowest average RMS was obtained using a larger interbed dispersivity. Near the former percolation ponds, the better match was obtained with a lower alluvium K_d of 2 mL/g, allowing more rapid transport from the former percolation ponds. This suggests that the geochemical parameters of the alluvium are probably spatially variable, and are influenced by historical water chemistry. The highest concentrations in the southern shallow perched water correspond to wells MW-15, and PW-1. Table J-12-8 suggests that the best match occurs with an interbed Kd of 22 mL/g, but the log10 RMS for that case is quite similar to the log10 RMS for the RI/BRA base case.

Table J-12-7. Southern shallow perched water calibration summary.

Simulation	Minimum Log10 RMS	Average Log10 RMS	Maximum Log10 RMS	Figure #
RI/BRA Model: Alluvial CEC=2 meq/100 g, Interbed K_d=50 mL/g	0.41	2.02	5.93	J-8-14
Geochemical Parameter Sensitivity				
Alluvial CEC of 3 meq/100 g, Interbed K_d=50 mL/g	0.48	1.69	4.94	J-10-6
Alluvial CEC of 7 meq/100 g, Interbed K_d=50 mL/g	0.46	3.04	7.61	J-10-21
Alluvial CEC of 2 meq/100 g, Interbed K_d=22 mL/g	0.38	1.40	5.12	J-10-32
Alluvial CEC of 2 meq/100 g, Interbed K_d=78 mL/g	0.44	1.91	5.18	J-10-43
Hydrologic Parameter Sensitivity				
Lower 3 cm/yr Infiltration through the tank farm Liner	0.40	1.86	5.45	J-11-6
Higher 39 cm/yr Infiltration through the tank farm Liner	0.41	2.02	5.93	J-11-18
Anthropogenic Water Losses Focused in Northern INTEC	0.42	2.09	6.03	J-11-29
Anthropogenic Water Losses Stopped in 2035	0.41	2.02	5.93	J-11-40
Larger Interbed Dispersivity	0.24	0.85	2.91	J-11-64

.

Table J-12-8. Southern shallow perched water calibration by well and simulation

Simulation	Well Name								
	MW-7-2	**MW-9-2**	**MW-15**	**PW-1**	**PW-2**	**PW-3**	**PW-4**	**PW-5**	**PW-6**
RI/BRA Model: Alluvial CEC=2 meq/100 g, Interbed K_d=50 mL/g	1.8906	2.7342	4.4428	0.4150	0.4419	1.2760	0.5257	0.5196	5.9285
Geochemical Parameter Sensitivity									
Alluvial CEC = 3 meq/100 g	2.3033	3.1876	4.9380	0.4772	0.5084	1.4541	0.5338	0.5467	1.2352
Alluvial CEC = 7 meq/100 g	3.5212	4.2381	7.6058	0.4585	0.9570	1.8999	0.5700	0.6443	7.4526
Interbed K_d = 22 mL/g	0.4311	1.3931	3.1297	0.4759	0.3815	0.7761	0.4194	0.4794	5.1165
Interbed K_d =78 mL/g	2.6291	3.4487	5.1785	0.4400	0.5376	1.5885	0.5367	0.5845	2.2346
Hydrologic Parameter Sensitivity									
Tank farm Liner Infiltration = 3 cm/yr	1.6451	2.4631	4.1690	0.4501	0.4047	1.1371	0.5194	0.5006	5.4470
Tank farm Liner Infiltration = 39 cm/yr	1.8912	2.7342	4.4434	0.4150	0.4420	1.2759	0.5257	0.5197	5.9284
Anthropogenic Water Losses Focused in Northern INTEC	1.9949	3.0018	4.5691	0.4210	0.4419	1.3012	0.5258	0.5200	6.0283
Anthropogenic Water Losses Stopped in 2035	1.8906	2.7342	4.4428	0.4150	0.4419	1.2760	0.5257	0.5196	5.9285
Larger Interbed Dispersivity	0.2439	0.7717	2.9065	0.7551	0.3572	0.9692	0.3389	0.4520	0.0000

J-12.3.5 Summary of Southern Deep Perched Water Calibration

The average log10 RMS in the northern shallow perched water ranges from 0.93 to 1.28 (Table J-12-9) for all simulations presented in this document. Weighting high and low concentration wells equally, the best match was obtained with the larger dispersivity. However, looking at all of the comparisons there is very little overall variability, with the exception of well 1807L (Table J-12-10). That well is furthest from the percolation ponds. Although the higher dispersivity results in the lowest log10 RMS in this region, it resulted in large underpredictions of concentrations in the northern upper shallow perched water. With this under consideration, the best match in the southern deep perched water occurs with an interbed K_d of 22 mL/g. This is indicative of the ionic strength of the percolation pond water decreasing the interbed K_d in the perched water bodies above this one.

Table J-12-9. Southern deep perched water calibration summary.

Simulation	Minimum Log10 RMS	Average Log10 RMS	Maximum Log10 RMS	Figure #
RI/BRA Model: Alluvial CEC=2 meq/100 g, Interbed K_d=50 mL/g	0.11	1.11	3.51	J-8-14
Geochemical Parameter Sensitivity				
Alluvial CEC of 3 meq/100 g, Interbed K_d=50 mL/g	0.05	1.15	3.53	J-10-6
Alluvial CEC of 7 meq/100 g, Interbed K_d=50 mL/g	0.01	1.28	3.62	J-10-21
Alluvial CEC of 2 meq/100 g, Interbed K_d=22 mL/g	0.05	1.00	3.03	J-10-32
Alluvial CEC of 2 meq/100 g, Interbed K_d=78 mL/g	0.04	1.24	3.90	J-10-43
Hydrologic Parameter Sensitivity				
Lower 3 cm/yr Infiltration through the tank farm Liner	0.26	1.12	3.50	J-11-6
Higher 39 cm/yr Infiltration through the tank farm Liner	0.12	1.11	3.51	J-11-18
Anthropogenic Water Losses Focused in Northern INTEC	0.26	1.05	3.52	J-11-29
Anthropogenic Water Losses Stopped in 2035	0.11	1.11	3.51	J-11-40
Larger Interbed Dispersivity	0.16	0.93	3.34	J-11-64

.

Table J-12-10. Southern deep perched water calibration by well and simulation

Simulation	Well Name					
	1804L	1804M	1807L	CS-CH	MW-1-4	MW-17-2
RI/BRA Model: Alluvial CEC=2 meq/100 g, Interbed K_d=50 mL/g	0.2608	0.4560	3.5149	0.1096	1.7136	0.6233
Geochemical Parameter Sensitivity						
Alluvial CEC = 3 meq/100 g	0.2549	0.4475	3.5336	0.0457	1.7624	0.8383
Alluvial CEC = 7 meq/100 g	0.2261	0.4244	3.6154	0.0118	1.9362	1.4486
Interbed K_d = 22 mL/g	0.3510	0.8915	3.0309	0.0511	1.3292	0.3738
Interbed K_d =78 mL/g	0.1229	0.4457	3.8953	0.0430	1.9146	1.0235
Hydrologic Parameter Sensitivity						
Tank farm Liner Infiltration = 3 cm/yr	0.2656	0.4610	3.5015	0.2629	1.7273	0.5009
Tank farm Liner Infiltration = 39 cm/yr	0.2608	0.4560	3.5149	0.1186	1.6786	0.6237
Anthropogenic Water Losses Focused in Northern INTEC	0.2601	0.4569	3.5164	0.8597	0.5064	0.6773
Anthropogenic Water Losses Stopped in 2035	0.2608	0.4560	3.5149	0.1096	1.7136	0.6233
Larger Interbed Dispersivity	0.2946	0.5556	3.3359	0.1572	0.8509	0.3568

J-13 DATA SUMMARY

Sodium-bearing waste released to the tank farm alluvium in 1972 was very acidic, contained high concentrations of sodium, aluminum, and nitrate, and contained 15,000 Ci of Sr-90. Because of the highly dynamic geochemical evolution of pore water chemistry as the released sodium-bearing waste migrated through the tank farm alluvium, a competitive cation exchange model was evaluated as a method to provide better estimates of Sr-90 migration. Existing data were used in this competitive cation exchange model of Sr-90 transport in the tank farm alluvium. Where data did not exist, various methods were used to estimate the likely range of values the missing data would fall within.

J-13.1 Review of Geochemical Data

J-13.1.1 Mineral Data

Large amounts of data exist on mineralogy and grain-size distribution of INTEC alluvium. Sufficient data exist to conclude that calcite will be present at about 5 volume% in the alluvium to neutralize the acid. The simulations show that there is a large excess of calcium over the amount needed to buffer the sodium-bearing waste, and so the simulations will not be sensitive to significant changes in this number.

There are quite a few analyses of cation exchange capacity that are representative of alluvium at INTEC. Samples analyzed for CEC by the USGS in 1956, and by DOE in 1965 are either representative of *in situ* alluvium or are supported by sufficient data to permit adjustment of the CEC values to be representative of alluvium. The range of CEC values from these two data sets is relatively small, 2 to 4.5 meq/100 g. Using the PHREEQC geochemical code, an inverse calculation was performed on measured alluvium Sr K_d values to estimate alluvium CEC. The range of estimated alluvium CEC values was from 1.5 to 14 meq/100 g, with all but a few values below 4 meq/100 g. This agreement indicates a very narrow range of plausible alluvium CEC.

Direct measurements of Sr K_d values have been made on sedimentary interbed samples collected at 110 ft, 140 ft, and 380 ft below land surface at INTEC. These K_d values range from 140 to 240 mL/g with a single outlier at 60 mL/g. Comparing the major cation chemistry of the water used in the laboratory experiments to that of the perched water at INTEC shows that the laboratory experiments were conducted using water much lower in divalent cations than the perched water. Because the divalent cations compete most strongly with strontium for cation exchange sites, these measured K_d values were deemed to be too high. PHREEQC was used to calculate revised K_d values by using actual perched water chemical analyses. These revised K_d values ranged from 20 to 100 mL/g with a midpoint near 50 mL/g. This range of K_d values is based on a range of CECs estimated from the Liszewski data between13 and 24 meq/100 g. Measured CEC values from the SDA interbeds range from 5 to 45 meq/100 g with an average of 21 meq/100 g, supporting these estimated CEC values.

J-13.1.2 Selectivity Data

Good agreement on the order of selectivity preference for cations for a wide range of materials presented by a number of authors indicates that selectivity coefficients should vary over a fairly narrow range and be primarily controlled by the identity of the cation, not by the sedimentary materials. No site-specific selectivity coefficients have been measured on INL or INTEC materials. Laboratory data collected by Hawkins and Short in 1965 provide data from a series of sorption experiments that was used to evaluate the ion exchange model for INTEC sediments. Sorption of Sr to INTEC alluvium is well explained by ion exchange on planar surfaces of clay minerals using selectivity coefficients from the literature. Based on the concurrence in the literature on the order of selectivity preference of cations for ion exchange, and the ability of the selectivity coefficients adopted from the literature to match the laboratory experiments of Hawkins and Short, we conclude that the selectivity coefficients from the literature are applicable to the INTEC alluvium.

J-14 OVERVIEW AND SUMMARY

Future contaminant concentrations in the SRPA at INTEC were predicted using a single base case. The RI/BRA base case used the most defensible geochemical and hydrologic parameters to estimate exposure concentrations for a future groundwater receptor. These model simulations were based upon an interbed K_d of 50 mL/g and an alluvium CEC of 2 meq/100 g, which resulted in 12,336 Ci of Sr-90 leaving the alluvium during the first 20 year following the CPP-31 release. The RI/BRA base case provides the standard against which to compare the effects of various geochemical and hydrologic parameters during the sensitivity analysis. The RI/BRA base case is also used for future risk predictions.

The RI/BRA base case relies on several parameters to predict future groundwater concentrations. Most notably, the following parameters have the biggest impact on model predictions:

- An effective infiltration rate of 18 cm/yr from precipitation derived from field observations was used. This accounts for 85% of the total annual precipitation (21 cm/yr) that occurs at INTEC. No sensitivity analysis was performed to evaluate the range of observed infiltration rates at INTEC. For example, a previously used value of 10 cm/yr was not evaluated.
- A cation exchange capacity of 2 meq/100 g was used that results in 12,336 Ci of Sr-90 having left the alluvium during the 20 years following the CPP-31 release. This accounts for approximately 75% of the total Sr-90 in the tank farm being released to the underlying perched water, which cannot be accounted for using current monitoring data. Using the results from the sensitivity analysis, SRPA concentrations are linearly proportional to the contaminant mass leaving the alluvium, and therefore, reducing the mass by 1/2 will result in reducing the predicted SRPA concentrations by 1/2.
- An effective alluvium Kd of 2 mL/g was calculated based on the predicted ratio of aqueous phase to solid phase Sr-90. This low Kd is sufficiently large that after 20 years, the Sr-90 remaining in the alluvium does not contribute significantly to aquifer contamination. However, the Kd of 2 mL/g is approximately one order of magnitude lower than measured values outside of the influence of CPP-31.
- Interbed adsorption is the single most sensitive parameter, and is dependant on water chemistry and inherent spatial variability associated with mineralogic heterogeneity. The RI/BRA model was based on a singe midrange value that allows prediction of the mean behavior. The range of potential SRPA concentrations was evaluated using bounding values of the adsorption coefficient resulting in predicted concentrations that either about equal to the MCL by 2095, or are significantly higher than the RI/BRA model predictions.
- In all parameterizations, the model consistently over-predicts the Sr-90 concentrations in the SRPA wells located near INTEC, generally by a factor of between 3 and 6, but in some cases by as much as an order of magnitude. This over-prediction of current Sr-90 concentrations in the aquifer will impact predictions of future concentrations, but more importantly, will affect the time the aquifer is predicted to be above MCLs.

Model results are summarized in Table J-14-1. The RI/BRA base case has predicted that the peak Sr-90 concentrations in the SRPA at 2095 will be 18.6 pCi/L and be less than the MCL by 2129. Predicted SRPA concentrations are predicted to range from 4 to 343 pCi/L with the majority of concentrations in the 10-21 pCi/L range. To understand this range, it is important to understand the geochemical and hydrologic influences upon the model.

J-14.1 Geochemical Influences

Geochemical variables evaluated in this study included parameters of the alluvium and interbeds (CEC, Sr-90 selectivity, and K_d), and the geochemistry of the pore water (Na concentrations). These parameters determine 1) how much Sr-90 leaves the alluvium in the initial rapid release from CPP-31, 2) the mobility of the Sr-90 remaining in the alluvium, 3) and the mobility of Sr-90 in the interbeds of the vadose zone. Figure J-14-1 shows that the activity leaving the alluvium is a nearly exponential function of the cation exchange capacity of alluvium. The range of CEC evaluated spans 2-15 meq/100 g, with the most plausible values ranging between 2-7 meq/100 g. throughout the entire range, the activity leaving the alluvium is fairly sensitive, and differs by roughly 10,000 Ci. However, within this CEC and release range, the resultant peak aquifer concentration only ranges between 10 and 19 pCi/L.

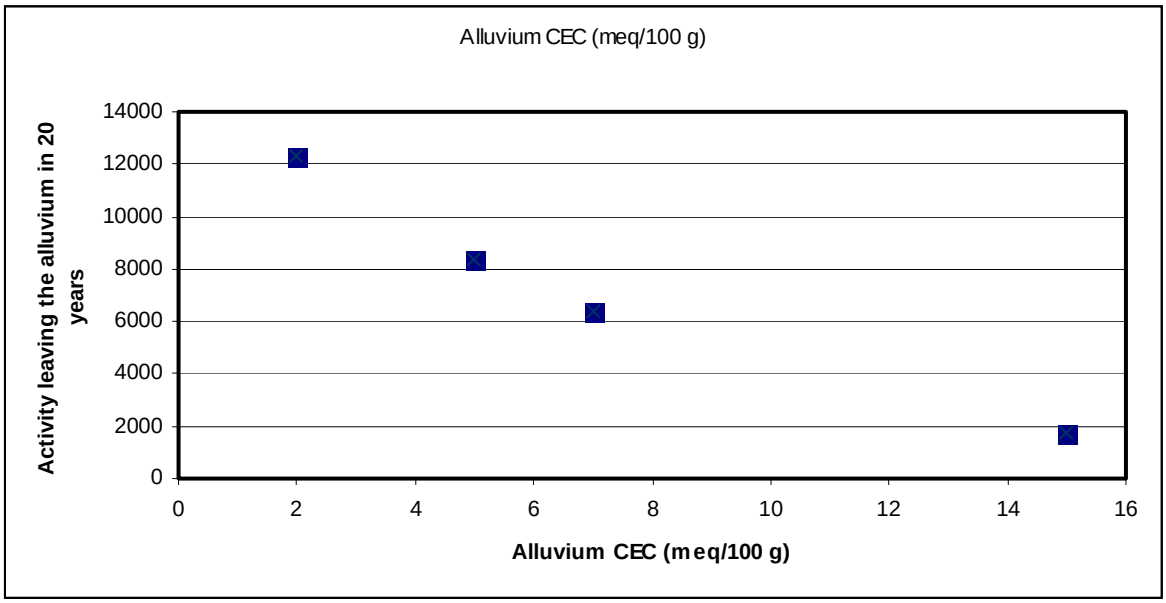

Figure J-14-1. Activity leaving the alluvium as a function of CEC.

As the released activity is removed from the alluvium through the cation exchange process, the remaining Sr-90 is held in place through a pseudo-steady state adsorption. Although more Sr-90 is predicted to remain in the alluvium at higher CEC, it is essentially immobile with a K_d approaching 50 mL/g as shown in Figure J-14-2. The most probable range of parameters places the K_d of residual alluvium Sr-90 in the 2-17 mL/g range, which is high enough to hold this remaining Sr-90 in the alluvium for an extended period of time. Table J-14-1 shows that the amount predicted to leave the alluvium at lower sodium concentrations falls within the range spanned by the plausible CEC range as does its effective K_d. This is also true for the range of Sr-90 selectivity coefficients simulated using the geochemical model. As a result, all of the sensitivity simulations evaluating alluvium geochemical characteristics fall within a fairly narrow range as shown in Figure J-14-3.

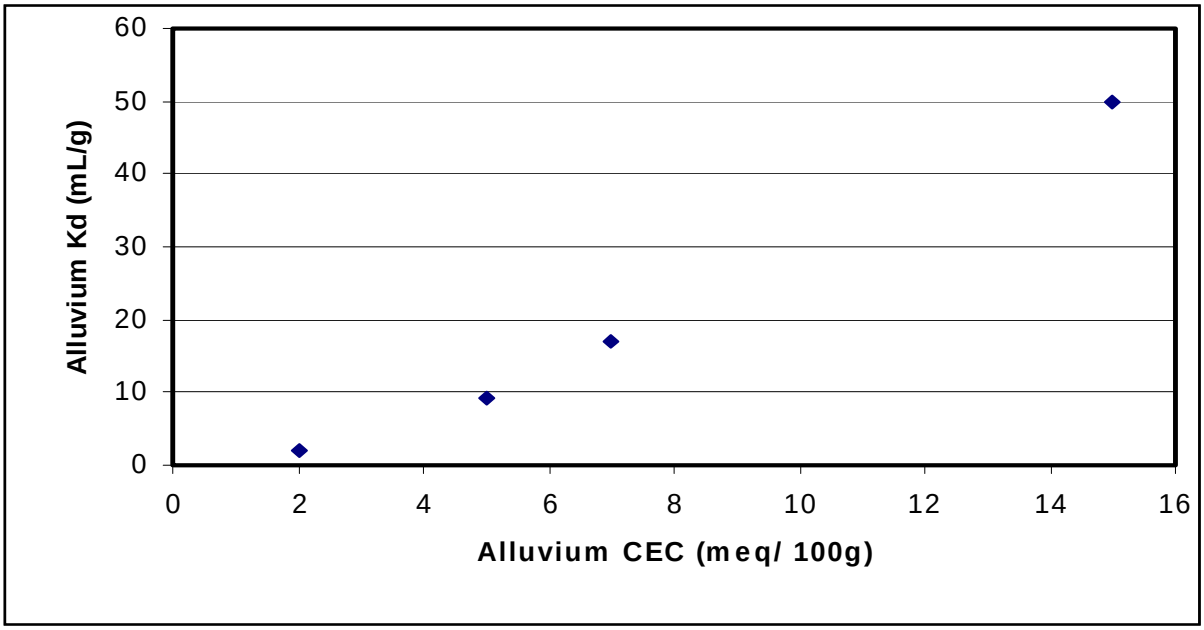

Figure J-14-2. Mobility of activity remaining in the alluvium as a function of CEC.

One of the outliers in the geochemical sensitivity study occurs in the simulation in which the interbed K_d was decreased to 22 mL/g (Figure J-14-3). This decrease affects not only the CPP-31 release, but also affects every other land-surface source of Sr-90. Sr-90 originating either from the OU 3-13 soil contamination, the failed injection well, or any of the OU 3-14 sources must pass through the interbeds in the vadose zone underlying INTEC. Because all of the sources are effected by adsorption in the interbeds, the K_d used to simulate transport through them is extremely important.Lowering the adsorption capacity affects peak aquifer concentrations by partitioning more of the Sr-90 into the aqueous phase off of the soils; by decreasing the travel time through the vadose zone and allowing less radioactive decay to occur; and by increasing the concentration gradients and resultant dispersive transport. In summary, the effects of interbed K_d are:

- The effective travel velocity is linearly proportional to the K_d: triple the K_d, triple the travel time.
- The half-life of Sr-90 is roughly 28 years. If the travel time is tripled, and given that the predicted time affected by peak aquifer concentrations is on the order of 200 years from now, the resultant residence time in the vadose zone is something like 600 years, or 20 half-lives.
- Aqueous concentrations are linearly proportional to the K_d, triple the K_d, cut the aqueous concentrations by one third.

Based on available data, a range of interbed K_ds is expected to span from 20-80 mL/g. At the low end (22 mL/g), the resultant concentration was predicted to be 110.8 pCi/L with concentrations remaining above the MCL through year 2263. At the high end, the resultant concentration would be 8.1 pCi/L with concentrations falling below the MCL by year 2096. Geochemical parameters used in the RI/BRA model were alluvium CEC=2 meq/100 g and interbed K_d=50 mL/g. Given these values, the peak concentration in the aquifer is predicted to be 18.5 pCi/L, and it falls below the MCL by 2129.

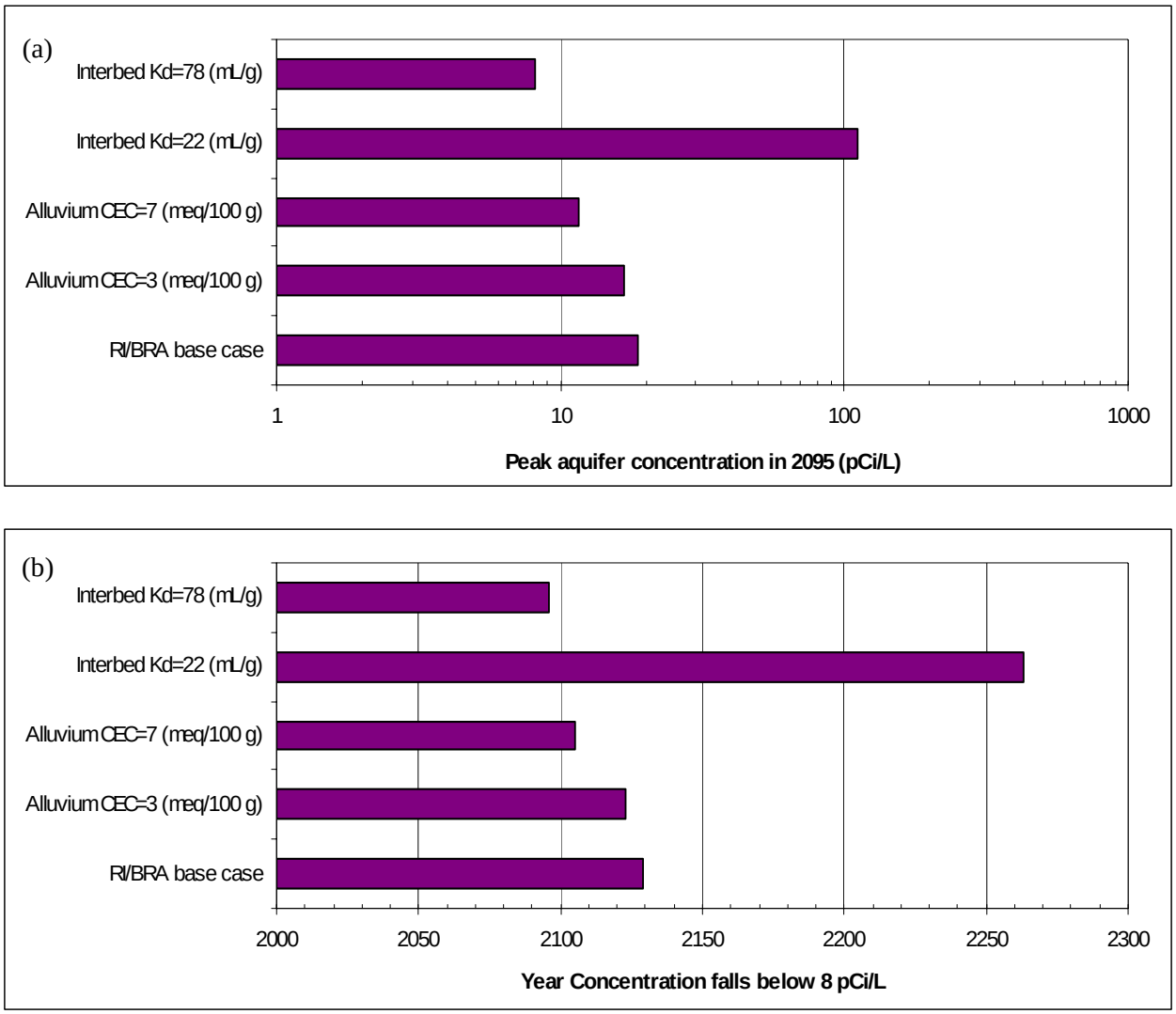

Figure J-14-3. Summary of geochemical sensitivity for the RI/BRA base case.

J-14.2 Hydrologic Influences

Hydrologic parameters studied here included infiltration rates through the tank farm, hydraulic characteristics of the interbeds, spatial distribution of unaccounted for anthropogenic water, and the land use scenario as impacted by the production wells. Figure J-14-4-A summarizes the predicted peak concentration and the year it falls below the MCL is summarized in Figure J-14-4-B. The highest peak value occurred when current estimates of the imbalance between pumped water and water discharges to the percolation ponds were focused near facilities in northern INTEC. The lowest value occurred when the dispersivity of the interbeds was increased in an effort to better match concentrations in CPP-55-06. Although increasing the dispersivity moved the Sr-90 out laterally, the predicted perimeter concentrations were much lower as a result of adsorption. As a result, the model underpredicted concentrations in wells with highest observed Sr-90 values. These two parameters also have the largest impact on the year during which the MCL is predicted to be exceeded. Of the two performance measures, the second is more sensitive overall. It is important because the time during which the MCL is exceeded dictates the duration of the remedial action. Sensitivity in this performance measure implies that cost estimates will also be subject to large uncertainty.

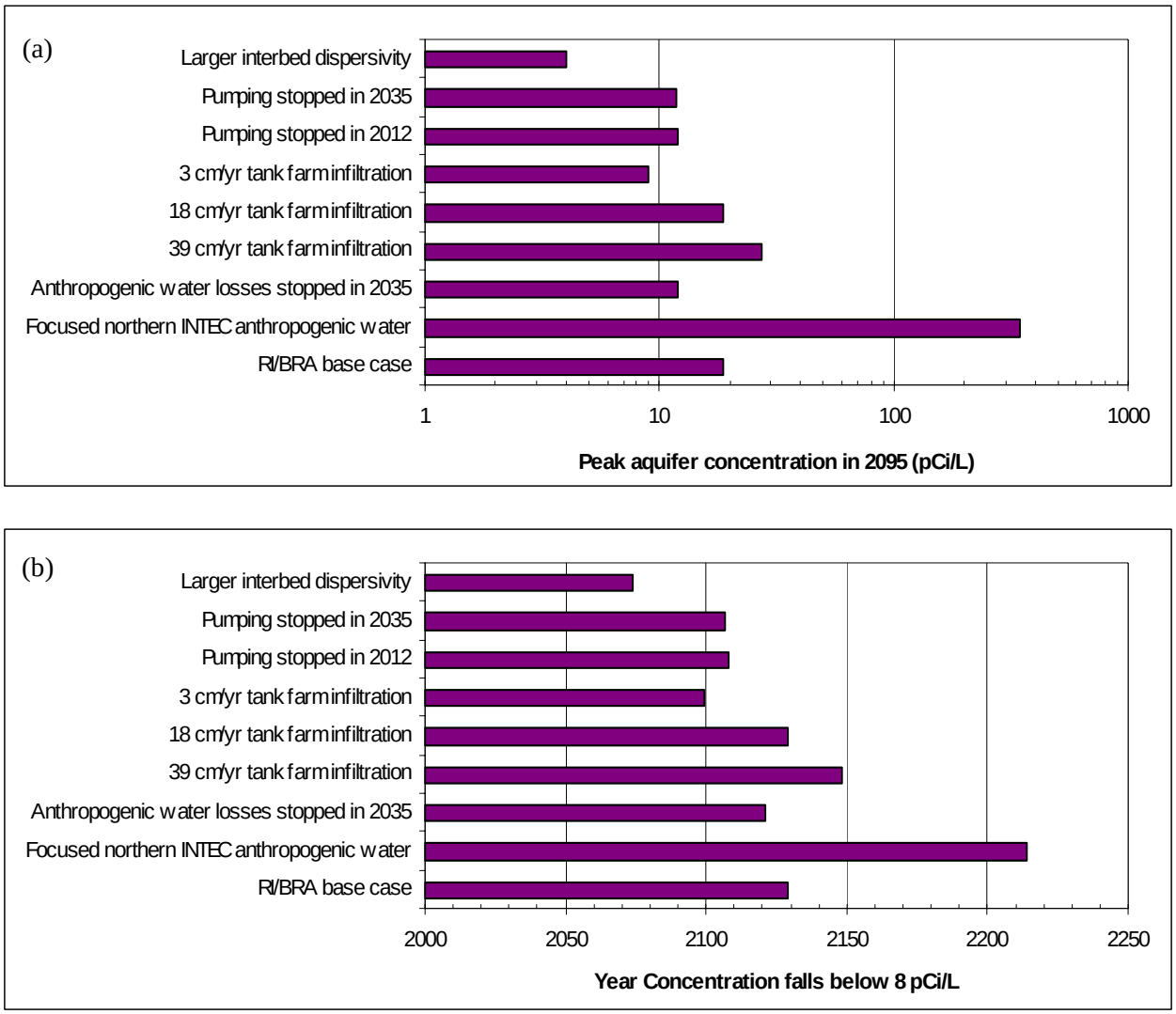

Figure J-14-4. Summary of hydrologic sensitivity for the RI/BRA base case.

Table J-14-1. Summary performance measures for all sensitivity simulations.

Simulation	Activity leaving alluvium within 20 years (Ci)	Activity remaining in alluvium at 20 years (Ci)	Effective K_d at 20 years (mL/g)	Peak Aquifer Concentration in 2095 (pCi/L)	Year C falls below 8 pCi/L
RI/BRA base case (CEC=2(meq/100 g)	**12336**	**3564**	**2**	**18.6**	**2129**
Geochemical Parameter Sensitivity Simulations					
Alluvium Properties					
CEC=3 (meq/100 g)	10864	5036	3.75	16.7	2123
CEC=5 (meq/100 g)	8380	7520	9.2		
CEC=7 (meq/100 g)	6403	9497	17	11.5	2105
$K_{Na/Sr}$=0.25	3378	12522	39		
$K_{Na/Sr}$=0.45	9480	6420	13		
Na^+ = 0.22 (mmol/L)	6517	9383			
Interbed adsorption coefficient					
K_d=22 (mL/g)	12336	3564	2	110.8	2263
K_d=78 (mL/g)	12336	3564	2	8.1	2096
Hydrologic Parameter Sensitivity Simulations					
Infiltration rate through tank farm liner (cm/yr)					
I=39	5580	10320	13	27.3	2148
I=18	12336	3564	2	18.6	2129
I=3	8037	7863	6.4	8.9	2099
Anthropogenic water					
Focused in Northern INTEC	12336	3564	2	343.0	2214
Losses Stopped in 2035	12336	3564	2	12.0	2121
Pumping Stopped in 2012	12336	3564	2	11.9	2108
Pumping Stopped in 2035	12336	3564	2	11.9	2107
Pumping Stopped in 2096	12336	3564	2	18.6	2108
Larger interbed dispersivity	12336	3564	2	4.0	2074

J-14.3 Summary

Important performance measures for evaluating the end state of Sr-90 are peak concentrations in 2095 and the time required for peak concentrations to be reduced below the MCL of 8 pCi/L. In all of the plausible parameters evaluated, we can conclude that:

- aquifer concentrations will exceed the MCL in 2095 in all but one of the RI/BRA results
- concentrations will exceed the MCL through year 2095, but will be below the MCL by 2263
- the predicted time frame that concentrations will exceed the MCL is very sensitive to interbed parameters
- the extent to which the MCL is exceeded is very sensitive to water chemistry and infiltration from anthropogenic water sources
- it is highly unlikely that the source of future aquifer contamination is from the Sr-90 that remains today in the alluvium
- it is believed that the existing contamination in the perched water and sorbed to the interbed that poses the greatest future risk.

J-15 REFERENCES

Appelo, C. A. J., 1994, "Cation and Proton Exchange, pH Variations, and Carbonate Reactions in a Freshening Aquifer," *Water Resources Research*, Vol. 30 (10), 2793-2805.

Appelo, C. A. J. and D. Postma, 1996, Geochemistry, Groundwater, and Pollution, A. A. Balkema, Rotterdam, Netherlands.

Barraclough, J. T., J. B. Robertson and V. J. Janzer, 1976, Hydrology of the Solid Waste Burial Ground, as Related to the Potential Migration of Radionuclides, Idaho National Engineering Laboratory, Open-File Report 76-471, IDO-22056, U. S. Geological Survey, Idaho Falls, Idaho, 1976, p.

Bartholomay, R. C., L. L. Knobel and L. C. Davis, 1989, *Mineralogy and Grain Size of Surficial Sediment from the Big List River Drainage and Vicinity, with Chemical and Physical Characteristics of Geologic Materials from Selected Sites at the Idaho National Engineering Laboratory, Idaho*, Open-File Report 89-384, DOE/ID-22081, U. S. Geological Survey, Idaho Falls, Idaho, July 1989, 74 p.

Bartholomay, R. C., 1990, *Mineralogical Correlation of Surficial Sediment from Area Drainages with Selected Sedimentary Interbeds at the Idaho National Engineering Laboratory, Idaho*, Water Resources Investigations Report 90-4147; DOE/ID-22092, U.S. Geological Survey, Idaho Falls, Idaho, 18p.

Bunde, R. L., J. Rosentreter, J. and M. J. Liszewski, 1998, "Rate of Strontium Sorption and the Effects of Variable Aqueous Concentrations of Sodium and Potassium on Strontium Distribution Coefficients of a Surficial Sediment at the Idaho National Engineering Laboratory," *Environmental Geology*, Vol. 34 (2/3), 135-142.

Bunde, R. L., J. Rosentreter, J., M. J. Liszewski, C. H. Hemming and J. Welhan, 1997, "Effects of Calcium and Magnesium on Strontium Distribution Coefficients," *Environmental Geology*, Vol. 32 (3), 219-229.

Del Debbio, J. A. and T. R. Thomas, 1989, *Transport Properties of Radionuclides and Hazardous Chemical Species in Soils at the Idaho Chemical Processing Plant*, WINCO-1068, Idaho National Engineering Laboratory, Westinghouse Idaho Nuclear Company, Idaho Falls, ID, October 1989, p.

DOE-ID, 2005, "Operable Unit 3-14 Tank Farm Soil and Groundwater Remedial Investigation /Baseline Risk Assessment (Draft)", DOE/NE-ID-11227, Rev. 0, U.S. Department of Energy Idaho Operations Office, May, 2005.

Hawkins, D. B. and D. C. Foster, 1963, *A Comparison of Two Methods of Sampling Gravel for the Evaluation of a Ground-Disposal Site for Radioactive Liquid Waste*, ID-12027, U. S. Atomic Energy Commission, Idaho Falls, ID, March 1963, 14 p.

Hawkins, D. B. and H. L. Short, 1965, *Equations for the Sorption of Cesium and Strontium on Soil and Clinoptilolite*, IDO-12046, U. S. Atomic Energy Commission, Idaho Falls, ID, November 1965, 33 p.

Hull, L. C., C. Grossman, R. A. Fjeld, J. T. Coates and A. W. Elzerman, 2004, "Hybrid Empirical - Theoretical Approach to Modeling Uranium Adsorption," *Applied Geochemistry*, Vol. 19 (5), 721-736.

ICP, 2004, *Evaluation of Tc-99 in Groundwater at INTEC: Summary of Phase 1 Results*, ICP/EXT-04-00244, Rev. 0, Idaho National Engineering and Enivronmental Laboratory, Idaho Completion Project, September 2004.

Leecaster, M. K. and L. C. Hull, 2003, *Spatial Distribution of Neptunium and Uranium Partition Coefficients (K_d) for Interbed Sediments at a Radioactive Waste Subsurface Disposal Area*, ICP/EXT-03-00088, Idaho Completion Project, Bechtel BWXT Idaho, Idaho Falls, ID, December 2003, 53 p.

Liszewski, M., J., J. J. Rosentreter, K. E. Miller and R. C. Bartholomay, 1998, *Strontium Distribution Coefficients of Surficial and Sedimentary Interbed Samples from the Idaho National Engineering and Environmental Laboratory, Idaho*, Water-Resources Investigation Report 98-4073, U. S. Geological Survey, Idaho Falls, ID, April 1998, 55 p.

Liszewski, M. J., J. Rosentreter, J. and K. E. Miller, 1997, *Strontium Distribution Coefficients of Surficial Sediment Samples from the Idaho National Engineering and Environmental Laboratory*, Water-Resources Investigations Report, 97-4044, U. S. Geological Survey, Idaho Falls, ID, 55 p.

Liszewski, M., J., J. J. Rosentreter, K. E. Miller and R. C. Bartholomay, 1998, Strontium Distribution Coefficients of Surficial and Sedimentary Interbed Samples from the Idaho National Engineering and Environmental Laboratory, Idaho, Water-Resources Investigation Report 98-4073, U. S. Geological Survey, Idaho Falls, ID, April 1998, 55 p.

McBride, M. B., 1994, Environmental Chemistry of Soils, Oxford University Press, New York.

Nace, R. L., M. Deutsch and P. T. Voegeli, 1956, *Geograph, Geology, and Water Resources of the National Reactor Testing Station, Idaho, Part 2: Geography and Geology*, IDO-22033-USGS, U. S. Geological Survey, Boise, ID, p.

Pace, M. N., J. J. Rosentreter and R. C. Bartholomay, 1999, Strontium Distribution Coefficients of Basalt and Sediment Infill Samples from the Idaho National Engineering and Environmental Laboratory, Idaho, Water Resources Investigations Report 99-4145, U. S. Geological Survey, Idaho Falls, ID, 56 p.

Reardon, E. J., 1981, "K_ds - Can They Be Used to Describe Reversible Ion Sorption Reactions in Contaminant Migration?" *Ground Water*, Vol. 19 (3), 279-286.

Rightmire, C. T., 1984, Description and Hydrogeologic Implications of Cored Sedimentary Material from the 1975 Drilling Program at the Radioactive Waste Management Complex, Idaho, Water-Resources Investigations Report 84-4071, DOE/ID-22067, U. S. Geological Survey, Idaho Falls, Idaho, June 1984, 33 p.

Roddy, M., 2005, *Geochemical Study for Perched Water Source Identification at INTEC*, EDF-5758, Rev 0, Idaho Cleanup Project, CH2M-WG Idaho LLC, Idaho Falls, ID, May 2005, 70 p.

Rosentreter, J., J., R. Nieves, J. Kalivas, J. P. Rousseau and R. C. Bartholomay, 1999, *The Use of Chemical and Physical Properties for Characterization of Strontium Distribution Coefficients at the Idaho National Engineering and Environmental Laboratory*, Water-Resources Investigations Report, 99-4123, U. S. Geological Survey, Idaho Falls, ID, 25 p.

Sparks, D. L., 2003, Environmental Soil Chemistry, Academic Press, Boston.

Steefel, C. I., S. Carroll, P. Zhao and S. Roberts, 2003, "Cesium Migration in Hanford Sediment: A Multisite Cation Exchange Model Based on Laboratory Transport Experiments," *Journal of Contaminant Hydrology*, Vol. 67 (1-4), 219-246.

Xu, T., E. Sonnenthal, N. Spycher and K. Pruess, 2004, *TOUGHREACT User's Guide: A Simulation Program for Non-Isothermal Multiphase Reactive Geochemical Transport in Variably Saturated Geologic Media*, LBNL-55460, Lawrence Berkeley National Laboratory, Berkeley, CA, May 2004, 192 p.

Zachara, J. M., S. C. Smith, C. X. Liu, J. P. McKinley, R. J. Serne and P. L. Gassman, 2002, "Sorption of Cs+ to Micaceous Subsurface Sediments from the Hanford Site, USA," *Geochemical Et Cosmochimica Acta*, Vol. 66 (2), 193-211.